Table 2 (continued)

No.	Conditioning[a]	GVHD prophylaxis, treatment	Transplant related toxicity	Symptoms[b] (post-transplant)	Acute GVHD	Chronic GVHD	Outcome (cause of death)
24	TBI (12G)/ CY(79)	CyA+MTX	Sepsis[f]	none	none	none	Dead, 9 months (Pneumococcal sepsis)

HSCT hematopoietic stem cell transplantation; *MRSA* methicillin-resistant Staphylococcus aureus; *PUVA* psoralen-ultraviolet A therapy; *TBI* total body irradiation; *BM* bone marrow (derived stem cells); *MSD* matched sibling donor; *URD* unrelated donor; *UCB* umbilical cord blood (derived stem cells); *MMFD* mismatched family donor; *PB* peripheral blood (derived stem cells);*ND* not done; *BU* busulfan; *CY* cyclophosphamide; *ATG* antithymocyte globulin; *FLU* fludarabine; *TNC* total nucleated cells; *MNC* mononuclear cell; *GVHD* graft versus host disease; *CyA* cyclosporin A; *MTX* methotrexate; *PSL* prednisolone; *mPSL* methylprednisolone; *MMF* mycophenolate moferil; *PRCA* pure red cell aplasia; *ARF* acute renal failure; *TMA* thrombotic microangiopathy; *EBV* Epstein-Barr virus, *AIHA* autoimmune hemolytic anemia

[a] The number in parentheses indicates the dose and units in Gy with TBI and mg/kg with the drugs

[b] Symptoms associated with XLT except petechiae

[c] Patient 10 had a reaction to ATG, therefore received only 1 dose instead of 3 doses

[d] Change to CyA due to renal dysfunction

[e] Extensive GVHD occurred during temporary cessation of GVHD prophylaxis due to renal dysfunction

[f] Prophylactic antibiotics were stopped after transplantation

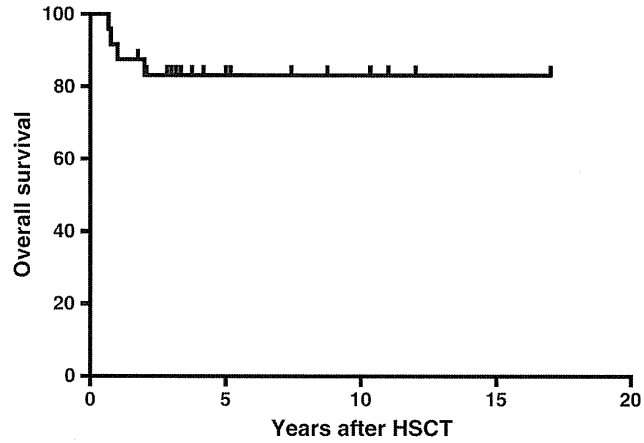

Fig. 1 Overall survival. Kaplan Meier estimate of survival probability of all study patients. | delineates a censored event

but 5 patients had platelet counts of $\geq 150\times10^3$ /μl (See Supplementary table 1). None had unusual bleeding tendency. Patient 14 who had become 100 % donor had a platelet count of 39×10^3 /μl, but no bleeding problems. Interestingly, his donor was a matched sister who was a carrier for the 559+5G>A mutation who had mild thrombocytopenia with a platelet count of 39×10^3 /μl [11]. The progressive IgA nephropathy affecting patients 19 and 20 improved clinically and by renal biopsy and both patients remained in remission at 3 and 13.5 years, respectively, after cessation of immunosuppressive therapy post transplantation [12]. The overall survival rate of our cohort was 83.3 %. Importantly, the patients recovered from pretransplant symptoms and transplantation related complications including GVHD and thrombotic microangiopathy. However, HSCT is not a benign procedure and may result in long-term complications such as chronic GVHD, infertility, or loss of the graft. In view of the excellent overall but unfavorable event-free survival of patients with XLT treated conservatively, it is imperative to address all aspects of HSCT before a decision is made for or against transplantation of patients with XLT. There are variables such as the experience of the transplant center, the health status of the patient, donor selection, conditioning regimen, and GVHD prophylaxis, the possibility of chronic GVHD, infertility, graft rejection. Our retrospective data analysis suggests that HSCT with myeloablative conditioning can be curative and considered a safe treatment option for XLT patients, and is not limited to patients<5 years of age, especially if an HLA identical sibling or a fully matched (9/10 or better) unrelated donor is available.

Acknowledgments The authors would like to thank the following Japanese physicians who contributed patient data to this study: H. Kanegane (Toyama); H. Kurosawa (Tochigi); A. Morimoto and T. Imamura (Kyoto); M Inoue (Osaka). This study was supported in part

by Japan's Ministry of Health, Labour and Welfare (to TM, SN), the DeJoria Wiskott-Aldrich Research Fund (to HDO) and by Biotest AG, Dreieich, Germany (to MHA).

Authorship Contributions K.O. and K.I. collected and analyzed data, and drafted the paper; K.I., H.D.O and S.N. designed and supervised research and revised the manuscript critically for important intellectual content; M.H.A. and L.D.N. submitted data, contributed to the interpretation of data, and revised the manuscript; and T.C.B., G.S., A.H.F., T.M., N.K, J.D., K.R.S., J.T.C. submitted data and contributed to interpretation of data. All authors participated sufficiently in the work to take public responsibility for the content, and gave final approval for publication.

Disclosure of Conflicts of Interest The authors have no conflict of interest to disclose.

References

1. Villa A, Notarangelo L, Macchi P, Mantuano E, Cavagni G, Brugnoni D, et al. X-linked thrombocytopenia and Wiskott-Aldrich syndrome are allelic diseases with mutations in the WASP gene. Nat Genet. 1995;9(4):414–7. doi:10.1038/ng0495-414.
2. Albert M, Notarangelo L, Ochs H. Clinical spectrum, pathophysiology and treatment of the Wiskott-Aldrich syndrome. Curr Opin Hematol. 2010. doi:10.1097/MOH.0b013e32834114bc.
3. Kobayashi R, Ariga T, Nonoyama S, Kanegane H, Tsuchiya S, Morio T, et al. Outcome in patients with Wiskott-Aldrich syndrome following stem cell transplantation: an analysis of 57 patients in Japan. Br J Haematol. 2006;135(3):362–6. doi:10.1111/j.1365-2141.2006.06297.x.
4. Ozsahin H, Cavazzana-Calvo M, Notarangelo L, Schulz A, Thrasher A, Mazzolari E, et al. Long-term outcome following hematopoietic stem-cell transplantation in Wiskott-Aldrich syndrome: collaborative study of the European Society for Immunodeficiencies and European Group for Blood and Marrow Transplantation. Blood. 2008;111(1):439–45. doi:10.1182/blood-2007-03-076679.
5. Moratto D, Giliani S, Bonfim C, Mazzolari E, Fischer A, Ochs H, et al. Long-term outcome and lineage-specific chimerism in 194 patients with Wiskott-Aldrich syndrome treated by hematopoietic cell transplantation in the period 1980–2009: an international collaborative study. Blood. 2011;118(6):1675–84. doi:10.1182/blood-2010-11-319376.
6. Albert M, Bittner T, Nonoyama S, Notarangelo L, Burns S, Imai K, et al. X-linked thrombocytopenia (XLT) due to WAS mutations: clinical characteristics, long-term outcome, and treatment options. Blood. 2010;115(16):3231–8. doi:10.1182/blood-2009-09-239087.
7. Imai K, Morio T, Zhu Y, Jin Y, Itoh S, Kajiwara M, et al. Clinical course of patients with WASP gene mutations. Blood. 2004;103(2):456–64. doi:10.1182/blood-2003-05-1480.
8. den Dunnen J, Antonarakis S. Nomenclature for the description of human sequence variations. Hum Genet. 2001;109(1):121–4. doi:10.1007/s004390100505.
9. Jin Y, Mazza C, Christie J, Giliani S, Fiorini M, Mella P, et al. Mutations of the Wiskott-Aldrich Syndrome Protein (WASP): hotspots, effect on transcription, and translation and phenotype/genotype correlation. Blood. 2004;104(13):4010–9. doi:10.1182/blood-2003-05-1592.
10. Otsubo K, Kanegane H, Nomura K, Miyawaki T, Ishizawa S. Atypical lymphoproliferative disorder in a patient with X-linked thrombocytopenia. Pediatr Blood Cancer. 2008;51(3):443–4. doi:10.1002/pbc.21644.
11. Inoue H, Kurosawa H, Nonoyama S, Imai K, Kumazaki H, Matsunaga T, et al. X-linked thrombocytopenia in a girl. Br J Haematol. 2002;118(4):1163–5. doi:10.1046/j.1365-2141.2002.03740.x.
12. Hoshino A, Shimizu M, Matsukura H, Sakaki-Nakatsubo H, Nomura K, Miyawaki T, et al. Allogeneic bone marrow transplantation appears to ameliorate IgA nephropathy in a patient with X-linked thrombocytopenia. J Clin Immunol. 2014;34(1):53–7. doi:10.1007/s10875-013-9964-4.

Published October 6, 2014, doi:10.4049/jimmunol.1401467

Two Novel Gain-of-Function Mutations of *STAT1* Responsible for Chronic Mucocutaneous Candidiasis Disease: Impaired Production of IL-17A and IL-22, and the Presence of Anti–IL-17F Autoantibody

Yasuhiro Yamazaki,* Masafumi Yamada,* Toshinao Kawai,† Tomohiro Morio,‡ Masafumi Onodera,† Masahiro Ueki,* Nobuyuki Watanabe,† Hidetoshi Takada,§ Shunichiro Takezaki,* Natsuko Chida,*,¶ Ichiro Kobayashi,* and Tadashi Ariga*

Heterozygous gain-of-function (GOF) mutations of *STAT1* are responsible for chronic mucocutaneous candidiasis disease (CMCD), one of the primary immunodeficiency diseases characterized by susceptibility to mucocutaneous *Candida* infection. To date, 30 aa changes have been reported: 21 in the coiled-coil domain and 9 in the DNA-binding domain. In this study, we report two novel *STAT1* GOF mutations of p.K278E in coiled-coil domain and p.G384D in DNA-binding domain in Japanese CMCD patients. Ectopic expression of these STAT1 mutants in HeLa cells was associated with increased phosphorylation of the mutant and the endogenous wild-type STAT1 due to impaired dephosphorylation, indicating heterodimers of the wild-type and mutant STAT1 cause impaired dephosphorylation, as did homodimers of the mutants. Because IL-17A production was not significantly reduced at least in one of the patients following PMA plus ionomycin stimulation, we further studied Th17-associated cytokines IL-17A, IL-17F, and IL-22 in response to more physiologically relevant stimulations. IL-17A and IL-22 production from PBMCs and CD4$^+$ cells was significantly reduced in four patients with *STAT1* GOF mutations, including the previously reported R274Q in response to anti-CD3 plus anti-CD28 Abs or *Candida* stimulations. In contrast, IL-17F production was comparable to healthy controls in response to anti-CD3 plus anti-CD28 Abs stimulation. These results indicate impaired production of IL-17A and IL-22 rather than IL-17F was associated with the development of CMCD in these patients. Additionally, only the anti–IL-17F autoantibody was detected in sera from 11 of 17 patients with *STAT1* GOF mutations, which may be useful as a marker for this disease.

***The Journal of Immunology*, 2014, 193: 000–000.**

Chronic mucocutaneous candidiasis (CMC) is characterized by susceptibility to *Candida* infection of the skin, nails, and mucosal membrane. CMC can occur as one of the various manifestations in patients with primary immunodeficiency diseases such as SCID, STAT3-deficient hyper-IgE syndrome (HIES), and autoimmune polyendocrine syndrome type 1 (APS1). Alternatively, CMC can be the only manifestation in patients with IL-17F deficiency, IL-17RA deficiency, or recently identified ACT1 deficiency (1, 2). This condition is described as isolated CMC or CMC disease (CMCD). Extensive analyses of CMCD patients resulting from impaired Th17 immunity have indicated the role of Th17 cells and Th17-associated cytokines in host defense against mucocutaneous *Candida* infection. In 2011, heterozygous *STAT1* mutations were reported as a cause of CMCD (3, 4), and since then, 30 aa changes have been reported: 21 in the coiled-coil domain (CCD) and 9 in the DNA-binding domain (DBD) (see Fig. 1A) (3–13). Accumulated data indicated these mutations account for around half of CMCD patients and were associated with gain of STAT1 function due to impaired dephosphorylation of STAT1 (4, 13). The development of CMCD in this disorder could be also attributable to impaired Th17 immunity (3, 4, 13, 14), although the precise mechanisms have not been elucidated.

In the present study, we describe two novel *STAT1* mutations of p.K278E and p.G384D in CCD and DBD, respectively, in three CMC patients. These mutations were associated with gain of STAT1 function due to impaired dephosphorylation of STAT1, but the proportion of IL-17A$^+$ cells was not significantly reduced in one of the patients after PMA plus ionomycin (IOM) stimulation. Thus, we further studied Th17-associated cytokines IL-17A, IL-17F, and IL-22 in response to more physiologically relevant stimulations (15) and found impaired production of IL-17A and IL-22 but not IL-17F. We also studied autoantibodies against Th17-associated cytokines in 17 patients with *STAT1* GOF mutations based on the facts that these patients manifest various autoimmune disorders (3, 4), and that patients with APS1 exhibiting various autoimmune disorders were shown to have neutral-

*Department of Pediatrics, Hokkaido University Graduate School of Medicine, Sapporo 060-8638, Japan; †Department of Human Genetics, National Center for Child Health and Development, Tokyo 157-8535, Japan; ‡Department of Pediatrics and Developmental Biology, Tokyo Medical and Dental University, Tokyo 113-8519, Japan; §Department of Pediatrics, Graduate School of Medical Sciences, Kyushu University, Fukuoka 812-8582, Japan; and ¶Department of Dentistry for Children and Disabled Persons, Hokkaido University Graduate School of Dental Medicine, Sapporo 060-8586, Japan

Received for publication June 9, 2014. Accepted for publication September 10, 2014.

This work was supported in part by a grant for Research on Intractable Diseases from the Japanese Ministry of Health, Labor, and Welfare.

Address correspondence and reprint requests to Dr. Masafumi Yamada, Department of Pediatrics, Hokkaido University Graduate School of Medicine, North 15 West 7, Kita-ku, Sapporo 060-8638, Japan. E-mail address: yamadam@med.hokudai.ac.jp

Abbreviations used in this article: ANA, anti-nuclear Ab; APS1, autoimmune polyendocrine syndrome type 1; CCD, coiled-coil domain; CD3/28, anti-CD3 plus anti-CD28 Abs; CMC, chronic mucocutaneous candidiasis; CMCD, chronic mucocutaneous candidiasis disease; DBD, DNA-binding domain; EGFP, enhanced GFP; GOF, gain-of-function; HIES, hyper-IgE syndrome; ILC, innate lymphoid cell; IOM, ionomycin; IP10, IFN-γ–inducible protein 10; LCL, lymphoid cell line; rh, recombinant human; WT, wild-type.

izing autoantibodies against various Th17-associated cytokines that could be associated with the development of CMC (16, 17). Patients with *STAT1* GOF mutations were demonstrated to have anti–IL-17F autoantibody, although no neutralizing activity was observed.

Materials and Methods

Patients

Patient 1 is a 20-y-old woman born to nonconsanguineous healthy Japanese parents. Recurrent oral thrush developed since the age of 1 y. She also had recurrent herpes zoster more than five times since the age of 4 y, and recurrent stomatitis about once every 2 mo that persisted around a week every time. *Candida* esophagitis developed at the age of 18 y. Impetigo contagiosa on the right thigh developed at the age of 19 y.

Patient 2 is a 35-y-old woman who had suffered from repetitive oral thrush and stomatitis since infancy. She had atopic dermatitis treated by anti-allergy drugs and topical corticosteroid. Bronchiectasis developed at the age of 18 y. Esophageal stenosis possibly caused by *Candida* esophagitis developed at the age of 19 y, which required balloon dilatation for swallowing foods. Iron-deficiency anemia had developed since her late 20s. She suffered from herpes zoster infection three times at the age of 11, 30, and 33 y.

Patient 3 is a 5-y-old boy who is a son of patient 2. He had oral thrush and onychomycosis, and was diagnosed as having CMC at the age of 1 y. Herpes zoster infection developed at the age of 4 y.

Patients 1, 2, and 3 had normal proportion of lymphocytes and their subsets with normal levels of serum γ-globulins. These 3 patients had not presented with endocrine diseases or autoimmune diseases.

Patient 4 is a 14-y-old boy with a heterozygous GOF mutation of p.T385M affecting the DBD of STAT1 as described previously (13). We studied patient 4 as a control to study the phosphorylation state of STAT1 GOF.

Patient 5 is an 18-y-old woman with a heterozygous GOF mutation of p.R274Q affecting the CCD of STAT1 as described previously (13). We studied patient 5 as a control to analyze Th17-associated cytokine production.

Informed consent for genetic analysis was obtained from the patients as well as normal controls under a protocol approved by the Institutional Review Board of Hokkaido University Hospital.

DNA isolation, PCR, and sequence analysis of PCR products

These procedures were performed following the methods described elsewhere (18).

Generation of EBV-transformed cell lines

EBV-transformed cell lines (EBV-lymphoid cell lines [LCLs]) were generated by in vitro transformation of human B cells with EBV (strain B95-8) as described elsewhere (18). Based on the results of *STAT1* sequence analysis, EBV-LCLs from patients 1, 3, and 4 with the heterozygous mutations of p.K278E, p.G384D, and p.T385M were designated as K278E/wild-type (WT), G384D/WT, and T385M/WT, respectively. Two EBV-LCLs from healthy controls were designated as WT1 and WT2.

Measurement of IFN-γ–inducible protein 10 concentration in supernatant of EBV-LCLs using cytometric bead array

This procedure was performed following the methods described elsewhere (13).

Transient transfection of plasmids expressing STAT1–enhanced GFP WT or mutants into HeLa cells

To evaluate the phosphorylation state of the ectopically expressed STAT1 and the endogenous WT STAT1 separately, we prepared the constructs expressing STAT1–enhanced GFP (EGFP) fusion protein, which was made by inserting WT *STAT1* cDNA into the pEGFP-N1 vector (BD Biosciences, Franklin Lakes, NJ) multicloning site. We generated *STAT1* mutants with K278E, G384D, or T385M by mutagenesis (PrimeSTAR mutagenesis basal kit, TaKaRa Bio, Shiga, Japan) following the manufacturer's protocol. HeLa cells were stripped by trypsin treatment 7 h before transfection and replaced at a density of 2.5×10^5 cells/ml in six-well plates. Plasmid DNA (5 μg/plate) carrying the WT or the various mutants or without *STAT1* alleles was used for cell transfection with the TransIT-LT1 reagent (Mirus Bio, Madison, WI). HeLa cells stimulated with recombinant human (rh)IFN-γ or rhIFN-α 36 h after transfection were harvested by trypsin. Transfection efficiencies were evaluated by FACSCalibur on the basis of the $EGFP^+$ cells.

Studies of STAT1 phosphorylation state and staurosporine treatment of cells

A total of 1×10^6 cells/ml EBV-LCLs in RPMI 1640 with 10% FBS or transfected HeLa cells as described above were stimulated with 1:1000 diluted rhIFN-γ (Shionogi, Osaka, Japan) for 30 min, or 1500 U/ml rhIFN-α (BioSource International, Camarillo, CA) for 15 min in 5% CO_2 at 37°C. For staurosporine treatment, these cells were then incubated with 1 μM staurosporine (Alomone Labs, Jerusalem, Israel), the tyrosine kinase inhibitor, in 0.5% DMSO final concentration for 15 min successively. The cells were harvested, and nuclear extracts obtained as described previously (13) were subjected to immunoblot analysis.

Immunoblot analysis for the studies of STAT1 phosphorylation state

This procedure was performed basically following the methods described previously with minor modification (13). Briefly, the SNAP i.d. 2.0 protein detection system (EMD Millipore, Billerica, MA) was used for the detection of STAT1, p-STAT1, and lamin A based on the manufactures protocols. All of the primary Abs were used at 1:2500 dilution. HRP-conjugated anti-mouse IgG secondary Ab (GE Healthcare, Buckinghamshire, U.K.) was used at 1:2500 dilution. The blots were then visualized by Luminata Forte Western HRP substrate (EMD Millipore).

Analysis of the production of IL-17A, IL-17F, IL-22, IFN-γ, and IL-4 from PBMCs and $CD4^+$ cells

PBMCs were recovered by centrifuging blood samples on Ficoll gradients. $CD4^+$ cells were positively selected by magnet sorting using CD4 microbeads (human) (Miltenyi Biotec, Auburn, CA) from PBMCs following the manufacturer's instructions. They were then adjusted to 1×10^6 cells/ml in RPMI 1640 containing 10% FBS. For stimulation with anti-CD3 plus anti-CD28 Abs (CD3/28), 1×10^6 cells/ml PBMCs were stimulated with 25 μl Dynabeads Human T-Activator CD3/28 (Life Technologies, Oslo, Norway) for 72 h. For *Candida* stimulation, PBMCs were stimulated with 100 μg/ml *Candida* Ag for skin test (Torii Pharmaceutical, Tokyo, Japan) for 72 h. $CD4^+$ cells were stimulated with 25 μl Dynabeads Human T-Activator CD3/28 for 1×10^6 cells/ml for 72 h, and 400 ng/ml PMA and 10 μg/ml IOM for 6 h. The concentration of IL-17A, IL-17F, IFN-γ, and IL-4 in the supernatant was measured with cytometric bead array (BD Biosciences) following the manufacturer's instructions. IL-22 was measured with a human IL-22 Quantikine ELISA kit (R&D Systems, Minneapolis, MN). Data from triplicate independent experiments are reported as the means ± SD. The p values were calculated with a Mann–Whitney U test. The purity of $CD4^+$ cells was examined with FACSCalibur using anti-human PE-Cy5–conjugated anti-CD4 Ab (BioLegend, San Diego, CA).

Flow cytometric analysis of intracellular IL-17A expression in $CD4^+$ cells

PBMCs at a density of 1×10^6 cells/ml were stimulated with 500 ng/ml PMA plus 5 μg/ml IOM for 6 h. We added of 10 μg/ml brefeldin A for the last 2 h. Harvested PBMCs were washed with TBST and stained with allophycocyanin-conjugated anti-human CD4 Ab (BioLegend) for 20 min. Cells were washed three times with PBS and fixed and permeabilized with a Foxp3 staining buffer set (eBioscience, San Diego, CA) for 20 min at 4°C. Cells were then washed three times and incubated for 30 min with PE-conjugated anti-human IL-17A (BioLegend). Cells were washed three times and analyzed with a BD LSRFortessa.

Detection of anti-cytokine autoantibodies in sera from patients by immunoblot analysis

Five hundred nanograms rhIL-17A, IL-17F, IL-22, IL-23, IL-1β, IL-6 (R&D Systems), IFN-α (BioSource International), and TGF-β1 (BioLegend) were separated by 15% polyacrylamide gels and transferred to Immobilon-P transfer membranes. The membranes were blocked by TBST with 5% non-fat skim milk for 1 h. They were then reacted with the sera at 1:1500 dilutions overnight at 4°C. The sera involved 17 STAT1 GOF CMC patients, 2 APS1 patients, 2 STAT3-deficient HIES patients, and 21 healthy controls. After washing four times with TBST, the membranes were incubated with HRP-conjugated goat anti-human IgG or IgA (Invitrogen, Frederick, MD) at 1:150,000 or 1:40,000 dilutions, respectively, in TBST with 5% non-fat skim milk for 1 h at 4°C. After washing four times, the blots were then visualized by ECL Select Western blotting detection reagent (GE Healthcare). To titrate anti–IL-17F autoantibody, we performed immunoblot analysis of sera from the patients serially diluted from 1:640 to 1:81,920.

Results

Two novel amino acid substitutions in STAT1

Direct sequence analysis demonstrated that patient 1 had a heterozygous base change of c.832A→G, p.K278E (K278E) in CCD, and the parents of patient 1 had WT sequence in *STAT1*. Both patients 2 and 3 had the heterozygous base change of c.1150G→A, p.G384D (G384D) in DBD of *STAT1* (Fig. 1A, 1B). These base changes have not been reported either as disease-causing mutations or as single nucleotide polymorphisms in the National Center for Biotechnology Information database, the Ensembl database, the Single Nucleotide Polymorphism Database, and the Human Genetic Variation Database, which have information on 1208 Japanese single nucleotide polymorphisms, or in our 100 controls without CMC (data not shown). Both K278E and G384D were evolutionarily conserved (Fig. 1C). K278E was predicted as tolerated by the sort intolerant from tolerant algorithm, and it was predicted as benign with a score of 0.011 (sensitivity, 0.96; specificity, 0.78) by the polymorphism phenotype-2 algorithm. G384D was predicted as tolerated by the sort intolerant from tolerant algorithm but was predicted as probably damaging by the polymorphism phenotype-2 algorithm with a score of 1.000 (sensitivity, 0.00; specificity, 1.00).

K278E and G384D were associated with STAT1 GOF and increased STAT1 phosphorylation after IFN-γ and IFN-α stimulation

Heterozygous *STAT1* GOF mutations were shown to be the genetic causes of autosomal dominant or sporadic CMC. The reported mutations were associated with increased STAT1 phosphorylation due to impaired dephosphorylation. First, to study whether the amino acid substitutions of K278E and G384D in STAT1 also lead to STAT1 GOF, the production of IFN-γ–inducible protein 10 (IP10), the downstream target of STAT1, was analyzed. IP10 production was significantly higher in K278E/WT and G384D/WT EBV-LCLs compared with healthy controls following IFN-γ stimulation (Fig. 2A). We then studied the STAT1 phosphorylation state in EBV-LCLs from the patients and controls. Expression of p-STAT1 following IFN-γ or IFN-α stimulation was higher in G384D/WT, K278E /WT, and T385M/WT than in WT1 EBV-LCLs (Fig. 2B, 2C). Ectopic expression of STAT1 mutants was associated with increased phosphorylation of the STAT1 mutants in HeLa cells (Fig. 2D). These results indicate that K278E and G384D are GOF mutations responsible for CMCD, and the mechanism of GOF is STAT1 hyperphosphorylation following the IFNs stimulations.

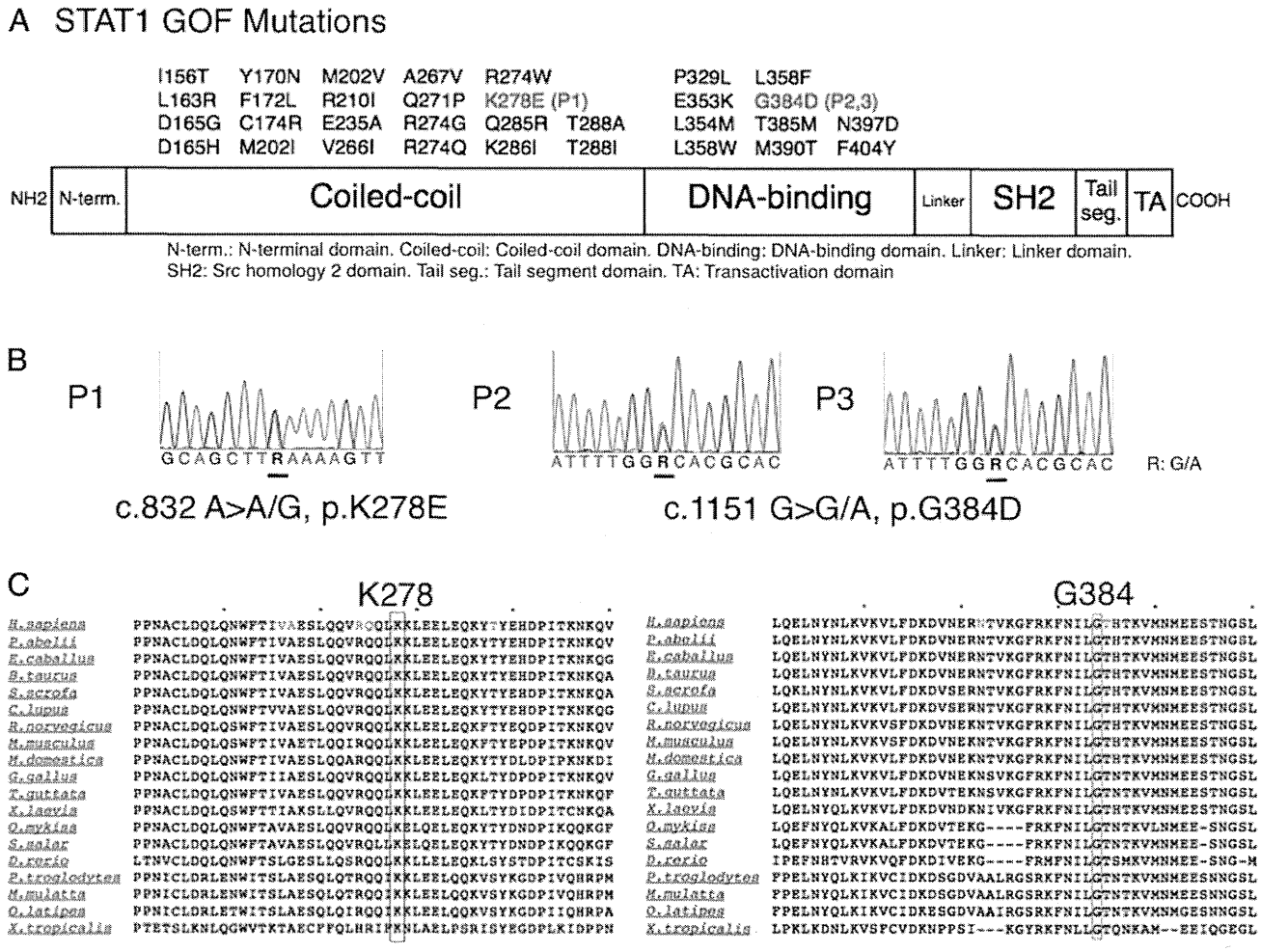

FIGURE 1. Two heterozygous base changes of *STAT1* leading to amino acid substitutions were identified in three CMCD patients. (**A**) The reported heterozygous *STAT1* mutations responsible for CMCD are shown. Mutations identified in this study are shown in red. (**B**) Direct sequence analysis of *STAT1* exon 10 in patient 1 (P1) and exon 14 in patients 2 (P2) and 3 (P3). Forward sequences are shown. (**C**) Comparison of the amino acid sequences of STAT1 in different species. The red rectangles indicate the amino acids corresponding to p.K278 or p.G384 in humans, respectively.

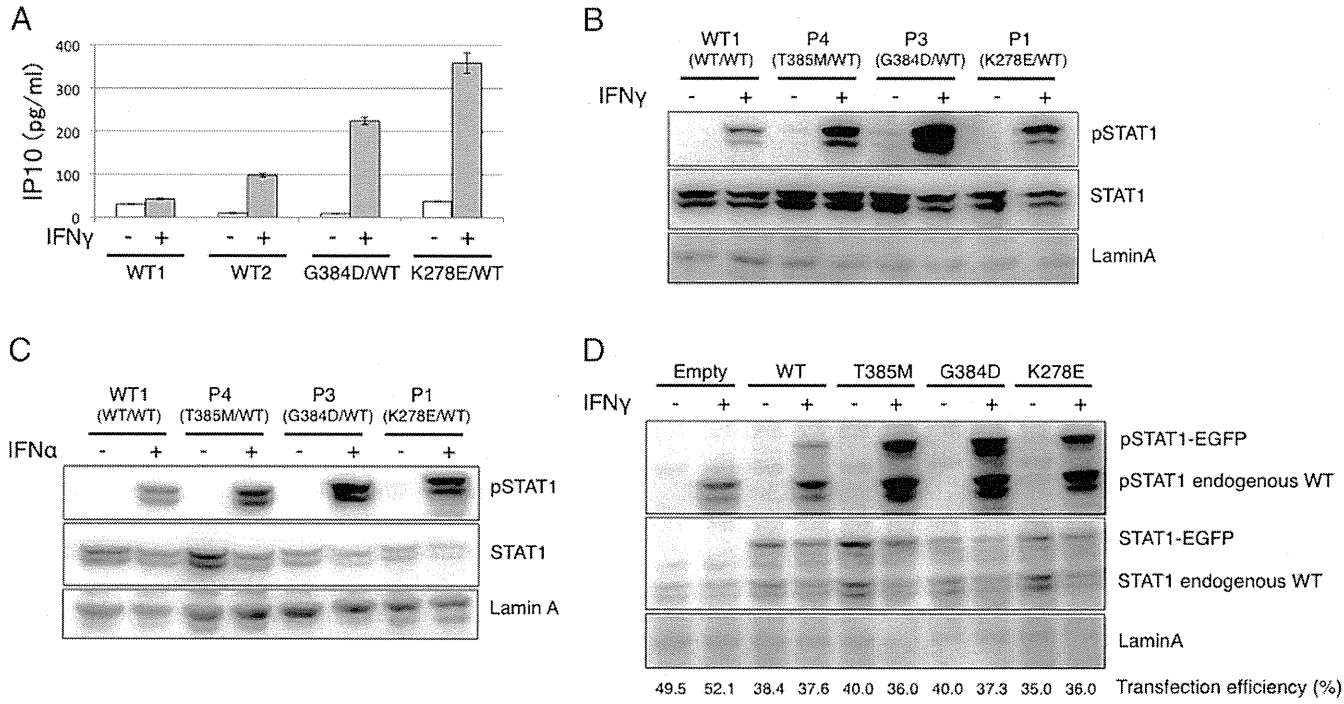

FIGURE 2. G384D and K278E were associated with GOF and increased phosphorylation of STAT1 in response to IFN-γ or IFN-α stimulation. (**A**) IP10 production from EBV-LCLs stimulated with or without IFN-γ for 6 h. (**B** and **C**) p-STAT1 and STAT1 expression in EBV-LCLs following IFN-γ stimulation for 30 min (B), and IFN-α stimulation for 15 min (C). (**D**) p-STAT1 and STAT1 expression in transfected HeLa cells following IFN-γ stimulation for 30 min. Transfection efficiencies were analyzed on the basis of GFP^+ cells and are described under each lane.

Increased phosphorylation of the STAT1 mutants was due to impaired dephosphorylation

The mechanisms underlying increased phosphorylation of the STAT1 mutants were further investigated with the tyrosine kinase inhibitor staurosporine. Dephosphorylation of the ectopically expressed STAT1-EGFP K278E or G384D mutants was impaired in HeLa cells following IFN-γ or IFN-α stimulation, compared with that of STAT1-EGFP WT (Fig. 3). Therefore, the mechanisms underlying increased STAT1 phosphorylation of K278E and G384D mutants involve impaired dephosphorylation of STAT1.

Increased phosphorylation and impaired dephosphorylation of the endogenous WT STAT1 in addition to the ectopically expressed mutants in HeLa cells

The endogenous WT STAT1 was also demonstrated to have increased STAT1 phosphorylation following IFN-γ stimulation when

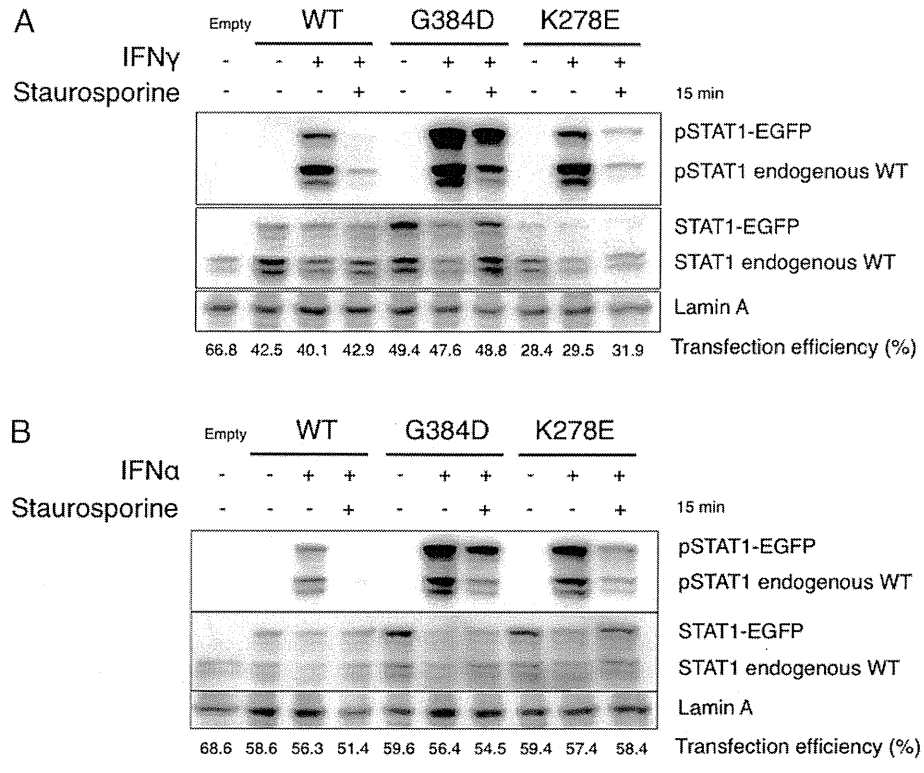

FIGURE 3. G384D and K278E were associated with increased phosphorylation of STAT1 due to impaired dephosphorylation. The p-STAT1 expression is shown in transfected HeLa cells first stimulated with IFN-γ for 30 min (**A**) or IFN-α for 15 min (**B**) followed by incubation with 1 μM staurosporine for 15 min. Transfection efficiencies are described under each lane.

either of the STAT1-EGFP mutants of K278E, G384D, and T385M was transiently transfected into HeLa cells (Fig. 2D). Moreover, impaired dephosphorylation was observed in the endogenous WT STAT1 when either of the STAT1-EGFP mutants was transiently expressed in HeLa cells (Fig. 3). Although these mechanisms were not fully elucidated in our study, they suggest that heterodimers of WT and the mutants of STAT1 could cause impaired dephosphorylation, as do homodimers of the STAT1 GOF mutants.

Th17 population was reduced in patients 1 and 3 but not in patient 2

Impaired differentiation of Th17 cells was indicated to be associated with the development of CMCD in patients with *STAT1* GOF mutations (3, 4, 13, 14). Therefore, we studied the proportion of $CD4^+IL\text{-}17A^+$ cells among $CD4^+$ cells in the patients with novel *STAT1* GOF mutations following PMA plus IOM stimulation for 6 h (Fig. 4). Patient 1 with a heterozygous K278E mutation and patient 3 with a heterozygous G384D mutation were shown to have relatively reduced $CD4^+IL\text{-}17A^+$ cells (0.28 and 0.24% of $CD4^+$ cells, respectively). In contrast, patient 2 with the same heterozygous G384D mutation as patient 3 had almost normal $CD4^+IL\text{-}17A^+$ cells (0.58% of $CD4^+$ cells). These findings prompted us to further study Th17-associated cytokines IL-17A, IL-17F, and IL-22 following various stimulations.

Evaluation of the profile of Th17-associated cytokine production

First, cytokine production was analyzed in the supernatant of the purified $CD4^+$ cells following PMA plus IOM stimulation for 6 h, the same stimulation as performed in evaluating Th17 population (Fig. 5). The purity of $CD4^+$ cells positively selected by CD4 microbeads was 97.5–99.7%. Production of the Th17-associated cytokines IL-17A, IL-17F, and IL-22 was not significantly reduced in the patients with *STAT1* GOF mutations compared with healthy controls. We then studied cytokine production after more physiologically relevant stimulations, that is, *Candida* or CD3/28 stimulations. Production of all the Th17-associated cytokines in PBMCs and $CD4^+$ cells was significantly reduced in response to *Candida* stimulation. Alternatively, although production of IL-17A and IL-22 was significantly reduced, IL-17F production was comparable to healthy controls following CD3/28 stimulation. Additionally, IFN-γ and IL-4, the principal cytokines of Th1 and Th2, respectively, were analyzed (Fig. 5). IFN-γ and IL-4 production from patients' PBMCs or $CD4^+$ cells was not significantly different from that of controls following *Candida* or CD3/28 stimulation. Each sample without stimulation showed nil or negligible cytokine production (data not shown).

Anti–IL-17F autoantibody was present in sera from CMC patients with STAT1 GOF

In 2010, two reports indicated the neutralizing Abs against IL-17A, IL-17F, and IL-22 would be the etiology of CMC in APS1 patients (16, 17). It is possible that CMCD in patients with *STAT1* GOF mutations could be also attributable to neutralizing Abs based on the fact that these patients often manifest autoimmune diseases. Thus, we analyzed autoantibodies against various cytokines, including Th17-associated cytokines, first with HRP-conjugated goat anti-human IgG Ab. Immunoblot analysis of sera from two APS1 patients showed various autoantibodies against Th17-associated cytokines in addition to IFN-α as reported previously (Fig. 6) (16, 17). We then studied sera from 17 STAT1 GOF patients and demonstrated the exclusive presence of anti–IL-17F IgG autoantibody (thereafter described as anti–IL-17F autoantibody) in 11 patients (64.7%) (Fig. 6). Two patients with STAT3-deficient HIES also showed anti–IL-17F autoantibody (Fig. 6). Immunoblot analysis of serially diluted sera from STAT1 GOF patients demonstrated that the titer of this autoantibody ranged from 1:2,560 to 1:20,480, and 1:2,560 was the most frequently observed (data not shown). Furthermore, with HRP-conjugated goat anti-human IgA Ab, anti–IL-17F IgA autoantibody was demonstrated in sera from six patients (P1, P6, P8–P11) who were all positive for anti–IL-17F autoantibody (data not shown). In contrast, none of the present patients was demonstrated to have autoantibodies against IL-1β, IL-6, and TGF-β1 that could be associated with Th17 differentiation (data not shown). Each of the anti–IL-17F, anti–IFN-α, and anti–IL-6 autoantibodies was detected in 1 among 21 healthy controls without any overlaps (Fig. 6 and data not shown).

We confirmed the results by more than two independent experiments.

Neutralizing activity was not demonstrated when IL-17F–induced IL-6 production was studied in healthy control fibroblasts in

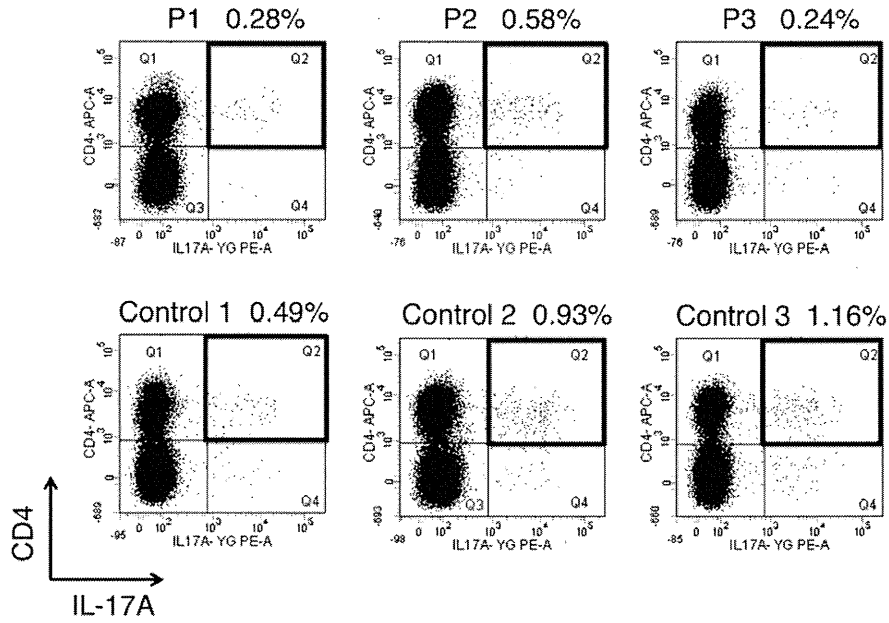

FIGURE 4. Patients 1 and 3 had reduced $CD4^+IL17A^+$ cells in response to PMA plus IOM stimulation, whereas patient 2 had a normal proportion of $CD4^+IL\text{-}17A^+$ cells compared with controls.

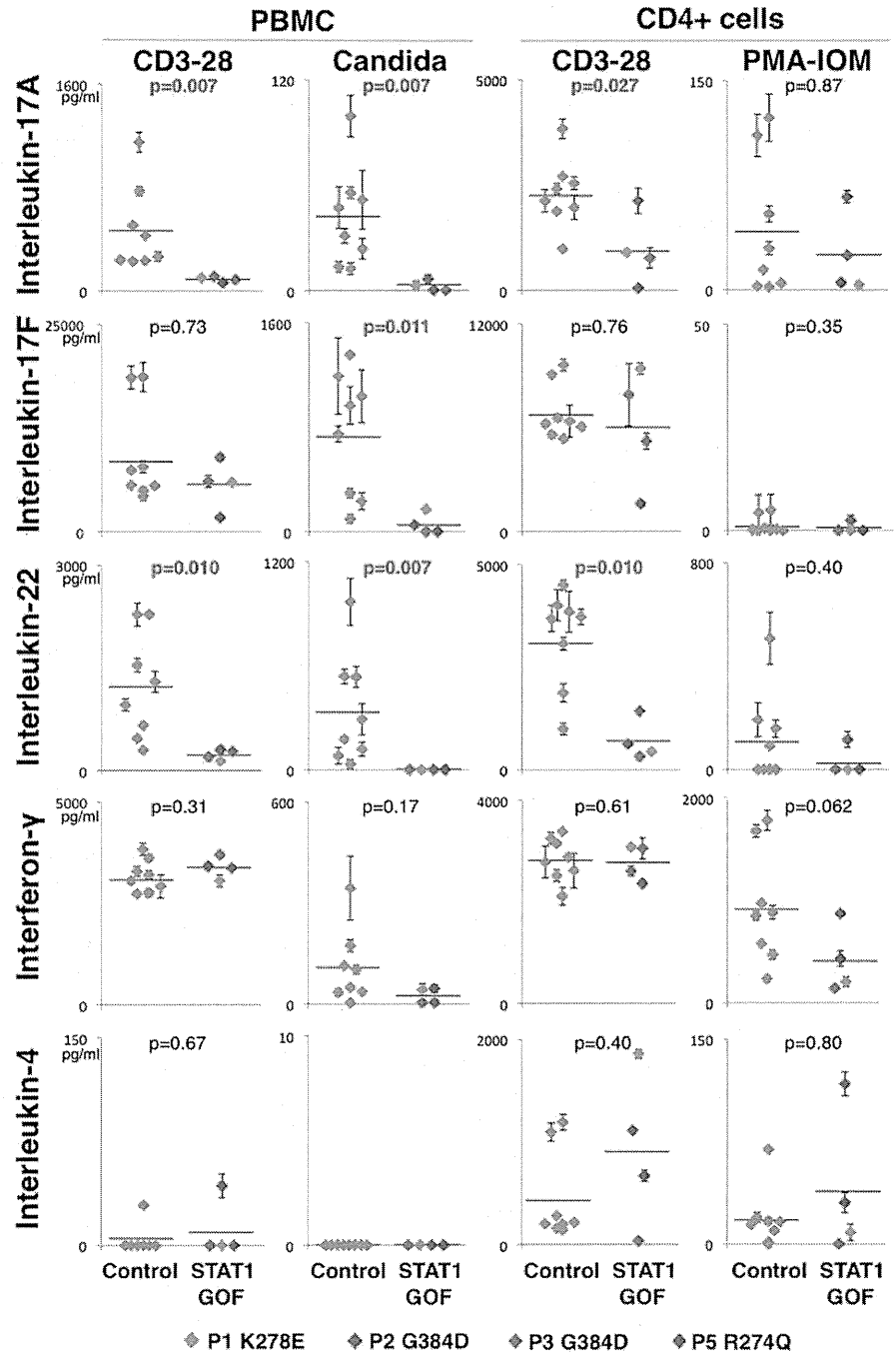

FIGURE 5. IL-17A and IL-22 production from PBMCs and $CD4^+$ cells was significantly reduced in four patients with STAT1 GOF in response to CD3/28 or *Candida* stimulations, whereas IL-17F production was comparable to healthy controls in response to CD3/28 stimulation. Productions of IL-17A, IL-17F, IL-22, IFN-γ, and IL-4 from PBMCs and $CD4^+$ cells of the patients with STAT1 GOF mutations are shown. Data from triplicate independent experiments are described as the means ± SD. The *p* values were calculated using a Mann–Whitney *U* test.

the presence of patients' sera (data not shown). This result may not completely exclude the possibility that the autoantibody has some neutralizing activity, because fairly high concentration of rhIL-17F (50 ng/ml) was required to induce significant IL-6 production from fibroblasts. Future studies are necessary to distinguish these possibilities.

We further addressed profiles of autoantibodies in the 17 patients with STAT1 GOF (Table I). Patients with anti–IL-17F autoantibody were more likely to have anti-nuclear Ab (ANA) or other autoantibodies, although information of more patients is needed.

Discussion

In this study we reported two novel heterozygous *STAT1* GOF mutations of K278E in CCD and G384D in DBD that are responsible for CMCD. These mutations were associated with increased STAT1 phosphorylation due to impaired dephosphorylation as observed in the previous reports (4, 13).

Extensive analyses of CMCD patients resulting from impaired Th17 immunity such as IL-17F deficiency or IL-17RA deficiency have indicated nonredundant roles of Th17 cells and Th17-associated cytokines in host defense against mucocutaneous *Candida* infection (1). The development of CMCD in patients with heterozygous *STAT1* GOF mutations was also indicated to be associated with impaired differentiation of Th17 cells (3, 4, 13, 14). However, a CMCD patient with a heterozygous *STAT1* GOF mutation of L163R was recently shown to have normal $CD4^+IL\text{-}17A^+$ cells, although in vitro Th17 differentiation was impaired (7). Our study also demonstrated that $CD4^+IL\text{-}17A^+$ cells were not remarkably reduced at least in patient 2 with a heterozygous *STAT1* GOF mutation of G384D (Fig. 4). These findings prompted us to speculate that susceptibility to CMCD in patients with *STAT1*

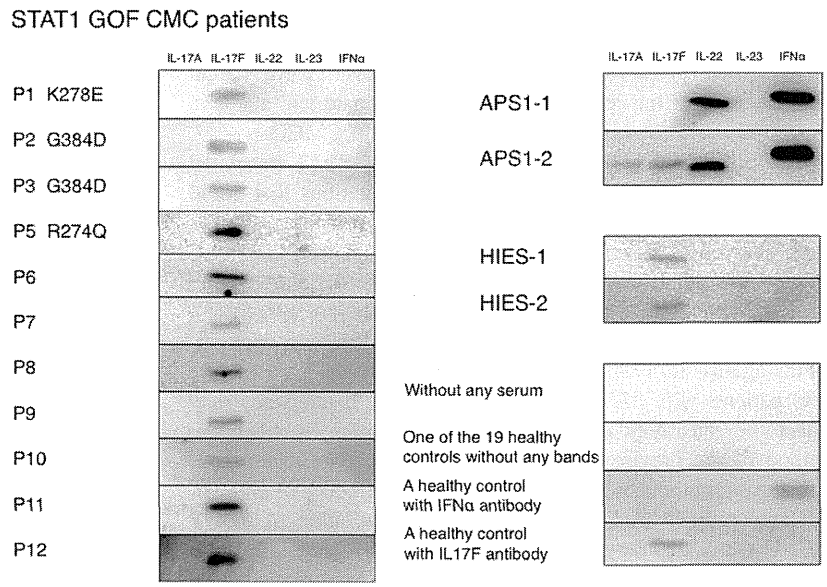

FIGURE 6. Immunoblot analysis showed the exclusive presence of anti–IL-17F autoantibody in the 11 of 17 STAT1 GOF patients' sera (64.7%). We confirmed the results by more than two independent experiments.

GOF mutations depends more on impaired production of other Th17-associated cytokines such as IL-17F or IL-22 than of IL-17A, which has been more extensively studied. ELISA and cytometric bead array studies unexpectedly revealed that production of IL-17F and IL-22 as well as IL-17A was not reduced in $CD4^+$ cells from the four patients with *STAT1* GOF mutations following PMA plus IOM stimulation. However, production of IL-17A and IL-22 but not IL-17F was significantly reduced in PBMCs or $CD4^+$ cells from these patients following more physiologically relevant stimulation of CD3/28. Therefore, it is possible that impaired production of IL-17A and IL-22 are more closely associated with the development of CMCD than of IL-17F in patients with *STAT1* GOF mutations in physiological conditions. Furthermore, production of IL-17A, IL-17F, and IL-22 from PBMCs was significantly reduced after *Candida* stimulation as observed in previous reports (3, 9), indicating that *Candida*-specific Th17 responses are impaired in patients with *STAT1* GOF mutations.

Whereas Th17 cells are widely accepted as the major IL-22 producers in the murine system (19–21), Th22 cells are suggested to be the major T cell subsets producing IL-22 in humans (22–24). Th22 cells are characterized by production of IL-22 with little or no IL-17, and they are important contributors to mucosal host defense. Thus, it is reasonable to think that deficient production of IL-22 from $CD4^+$ cells in the present patients was attributable to impaired Th22 differentiation and/or response, although it was not confirmed in this study.

Moreover, subsets of innate lymphoid cells (ILCs) recently identified in mice and humans are restricted to mucosal tissues and react promptly to acute bacterial or fungal infection (25). IL-17–producing ILC3, including lymphoid tissue inducer cells, produces IL-17 and IL-22, and IL-22–producing ILC3 produces only IL-22 (26). Recent studies indicate that ILC3 provides a rapid source of Th17-associated cytokines that is essential for early host protection, and Th17 or Th22 cells in turn become the dominant source of these cytokines that is required for complete clearance

Table I. Profiles of autoantibodies in the 17 patients with STAT1 GOF

Patient	Positive Autoantibodies	Negative Autoantibodies	αIL17F
1	ANA 160×, microsome 100×, TRAb 1.0 (< 0.9 IU/l)	TgAb	+
2		ANA, dsDNA, TRAb, TPO, TgAb, GAD, IAA, direct Coombs test	+
3	dsDNA 10 (<10 IU/ml)	ANA, TRAb, TPO, TgAb, GAD, IAA, direct Coombs test	+
4	TRAb (blocking rate 16% [<15%])	ANA	−
5	TgAb 55.33 (<40 IU/ml)	ANA, dsDNA, TRAb, TPO, GAD, IAA, IA-2, CCP, RF, c-ANCA, p-ANCA, AMA, αPL	+
6	ANA 160×	TPO, TgAb	+
7	Direct and indirect Coombs test	ANA, TRAb	+
8	ANA 40×	TPO, TgAb	+
9	ANA 40×	dsDNA, TPO, TgAb, GAD, IAA, IA-2	+
10	ANA 40×	dsDNA, TPO, TgAb	+
11	ANA 80×	TRAb	+
12		ANA, GAD, IAA, IA-2	+
13		ANA, TPO, TgAb	−
14		ANA, TRAb	−
15		ANA, TPO, TgAb, ASMA	−
16		ANA, TPO, TgAb	−
17		ANA	−

AMA, anti-mitochondrial Ab; ASMA, anti–smooth muscle Ab; c-ANCA, proteinase 3–anti-neutrophil cytoplasmic Ab; CCP, anti–cyclic citrullinated peptide Ab; dsDNA, anti-dsDNA Ab; GAD, anti–glutamic acid decarboxylase Ab; IA-2, anti-insulinoma–associated protein-2 Ab; IAA, insulin autoantibody; αIL17F, anti–IL-17F autoantibody; microsome, anti-microsomal Ab; p-ANCA, myeloperoxidase–anti-neutrophil cytoplasmic Ab; αPL, anti-phospholipid Ab; RF, rheumatoid factor; TgAb, anti-thyroglobulin Ab; TPO, anti–thyroid peroxidase Ab; TRAb, TSH receptor Ab.

of infection (26). Although genetic causes of CMCD have been associated with defects of Th17 immunity, they may also affect innate sources of IL-17 or IL-22. Future studies may provide an understanding of the relative contribution of innate and adaptive sources of these cytokines to the development of CMCD.

We further studied autoantibodies against Th17-associated cytokines in 17 patients with *STAT1* GOF mutations that could be associated with the development of CMCD. Autoantibodies were detected exclusively against IL-17F in sera from 11 of 17 patients and additionally 2 HIES patients (Fig. 6), although no neutralizing activity was observed. This result is in contrast with the previous report by Liu et al. (4) addressing that no autoantibodies against IL-17A, IL-17F, and IL-22 were detected in sera from patients with *STAT1* GOF mutations. The discrepancy may reflect the sensitivity of each assay system used, although the method of the previous study was not shown. One recent case report using immunoblot analysis showed the presence of anti–IL-17F autoantibody in a patient with R274Q mutation of *STAT1* (27). These results may indicate that anti–IL-17F autoantibody is useful as a marker for CMC, although the presence of this autoantibody may not be associated with the development of CMC.

Note that the expression of STAT1 GOF mutants was associated with impaired dephosphorylation of the endogenous WT STAT1 as well as the mutants themselves following the IFNs stimulation (Fig. 3). To our knowledge, this finding has not been reported because U3C cells deficient for endogenous STAT1 expression were used in the previous studies. Our results indicate that impaired dephosphorylation is present in heterodimers of WT STAT1 and GOF mutants as well as homodimers of the GOF mutants.

Acknowledgments

We thank the patients and their families for the collaboration in this study.

Disclosures

The authors have no financial conflicts of interest.

References

1. Puel, A., S. Cypowyj, J. Bustamante, J. F. Wright, L. Liu, H. K. Lim, M. Migaud, L. Israel, M. Chrabieh, M. Audry, et al. 2011. Chronic mucocutaneous candidiasis in humans with inborn errors of interleukin-17 immunity. *Science* 332: 65–68.
2. Boisson, B., C. Wang, V. Pedergnana, L. Wu, S. Cypowyj, M. Rybojad, A. Belkadi, C. Picard, L. Abel, C. Fieschi, et al. 2013. An ACT1 mutation selectively abolishes interleukin-17 responses in humans with chronic mucocutaneous candidiasis. *Immunity* 39: 676–686.
3. van de Veerdonk, F. L., T. S. Plantinga, A. Hoischen, S. P. Smeekens, L. A. Joosten, C. Gilissen, P. Arts, D. C. Rosentul, A. J. Carmichael, C. A. Smits-van der Graaf, et al. 2011. STAT1 mutations in autosomal dominant chronic mucocutaneous candidiasis. *N. Engl. J. Med.* 365: 54–61.
4. Liu, L., S. Okada, X. F. Kong, A. Y. Kreins, S. Cypowyj, A. Abhyankar, J. Toubiana, Y. Itan, M. Audry, P. Nitschke, et al. 2011. Gain-of-function human STAT1 mutations impair IL-17 immunity and underlie chronic mucocutaneous candidiasis. *J. Exp. Med.* 208: 1635–1648.
5. Lee, P. P., H. Mao, W. Yang, K. W. Chan, M. H. Ho, T. L. Lee, J. F. Chan, P. C. Woo, W. Tu, and Y. L. Lau. 2014. *Penicillium marneffei* infection and impaired IFN-gamma immunity in humans with autosomal-dominant gain-of-phosphorylation STAT1 mutations. *J. Allergy Clin. Immunol.* 133: 894–896.e5.
6. Romberg, N., H. Morbach, M. G. Lawrence, S. Kim, I. Kang, S. M. Holland, J. D. Milner, and E. Meffre. 2013. Gain-of-function STAT1 mutations are associated with PD-L1 overexpression and a defect in B-cell survival. *J. Allergy Clin. Immunol.* 131: 1691–1693.
7. Mekki, N., I. Ben-Mustapha, L. Liu, L. Boussofara, S. Okada, S. Cypowyj, N. Ghariani, W. Saidi, M. Denguezli, J. L. Casanova, et al. 2014. IL-17 T cells' defective differentiation in vitro despite normal range ex vivo in chronic mucocutaneous candidiasis due to STAT1 mutation. *J. Invest. Dermatol.* 134: 1155–1157.
8. Sampaio, E. P., A. P. Hsu, J. Pechacek, H. I. Bax, D. L. Dias, M. L. Paulson, P. Chandrasekaran, L. B. Rosen, D. S. Carvalho, L. Ding, et al. 2013. Signal transducer and activator of transcription 1 (STAT1) gain-of-function mutations and disseminated coccidioidomycosis and histoplasmosis. *J. Allergy Clin. Immunol.* 131: 1624–1634.
9. Soltész, B., B. Tóth, N. Shabashova, A. Bondarenko, S. Okada, S. Cypowyj, A. Abhyankar, G. Csorba, S. Taskó, A. K. Sarkadi, et al. 2013. New and recurrent gain-of-function STAT1 mutations in patients with chronic mucocutaneous candidiasis from Eastern and Central Europe. *J. Med. Genet.* 50: 567–578.
10. Mizoguchi, Y., M. Tsumura, S. Okada, O. Hirata, S. Minegishi, K. Imai, N. Hyakuna, H. Muramatsu, S. Kojima, Y. Ozaki, et al. 2014. Simple diagnosis of STAT1 gain-of-function alleles in patients with chronic mucocutaneous candidiasis. *J. Leukoc. Biol.* 95: 667–676.
11. Aldave, J. C., E. Cachay, L. Núñez, A. Chunga, S. Murillo, S. Cypowyj, J. Bustamante, A. Puel, J. L. Casanova, and A. Koo. 2013. A 1-year-old girl with a gain-of-function STAT1 mutation treated with hematopoietic stem cell transplantation. *J. Clin. Immunol.* 33: 1273–1275.
12. Al Rushood, M., C. McCusker, B. Mazer, R. Alizadehfar, B. Grimbacher, M. Depner, and M. Ben-Shoshan. 2013. Autosomal dominant cases of chronic mucocutaneous candidiasis segregates with mutations of signal transducer and activator of transcription 1, but not of Toll-like receptor 3. *J. Pediatr.* 163: 277–279.
13. Takezaki, S., M. Yamada, M. Kato, M. J. Park, K. Maruyama, Y. Yamazaki, N. Chida, O. Ohara, I. Kobayashi, and T. Ariga. 2012. Chronic mucocutaneous candidiasis caused by a gain-of-function mutation in the STAT1 DNA-binding domain. *J. Immunol.* 189: 1521–1526.
14. Smeekens, S. P., T. S. Plantinga, F. L. van de Veerdonk, B. Heinhuis, A. Hoischen, L. A. Joosten, P. D. Arkwright, A. Gennery, B. J. Kullberg, J. A. Veltman, et al. 2011. STAT1 hyperphosphorylation and defective IL12R/IL23R signaling underlie defective immunity in autosomal dominant chronic mucocutaneous candidiasis. *PLoS ONE* 6: e29248.
15. Trickett, A., and Y. L. Kwan. 2003. T cell stimulation and expansion using anti-CD3/CD28 beads. *J. Immunol. Methods* 275: 251–255.
16. Puel, A., R. Döffinger, A. Natividad, M. Chrabieh, G. Barcenas-Morales, C. Picard, A. Cobat, M. Ouachée-Chardin, A. Toulon, J. Bustamante, et al. 2010. Autoantibodies against IL-17A, IL-17F, and IL-22 in patients with chronic mucocutaneous candidiasis and autoimmune polyendocrine syndrome type I. *J. Exp. Med.* 207: 291–297.
17. Kisand, K., A. S. Bøe Wolff, K. T. Podkrajsek, L. Tserel, M. Link, K. V. Kisand, E. Ersvaer, J. Perheentupa, M. M. Erichsen, N. Bratanic, et al. 2010. Chronic mucocutaneous candidiasis in APECED or thymoma patients correlates with autoimmunity to Th17-associated cytokines. *J. Exp. Med.* 207: 299–308.
18. Yamada, M., Y. Okura, Y. Suzuki, S. Fukumura, T. Miyazaki, H. Ikeda, S. Takezaki, N. Kawamura, I. Kobayashi, and T. Ariga. 2012. Somatic mosaicism in two unrelated patients with X-linked chronic granulomatous disease characterized by the presence of a small population of normal cells. *Gene* 497: 110–115.
19. Wolk, K., K. Warszawska, C. Hoeflich, E. Witte, S. Schneider-Burrus, K. Witte, S. Kunz, A. Buss, H. J. Roewert, M. Krause, et al. 2011. Deficiency of IL-22 contributes to a chronic inflammatory disease: pathogenetic mechanisms in acne inversa. *J. Immunol.* 186: 1228–1239.
20. Volpe, E., N. Servant, R. Zollinger, S. I. Bogiatzi, P. Hupé, E. Barillot, and V. Soumelis. 2008. A critical function for transforming growth factor-β, interleukin 23 and proinflammatory cytokines in driving and modulating human T_H-17 responses. *Nat. Immunol.* 9: 650–657.
21. Liu, Y., B. Yang, M. Zhou, L. Li, H. Zhou, J. Zhang, H. Chen, and C. Wu. 2009. Memory IL-22-producing $CD4^+$ T cells specific for *Candida albicans* are present in humans. *Eur. J. Immunol.* 39: 1472–1479.
22. Duhen, T., R. Geiger, D. Jarrossay, A. Lanzavecchia, and F. Sallusto. 2009. Production of interleukin 22 but not interleukin 17 by a subset of human skin-homing memory T cells. *Nat. Immunol.* 10: 857–863.
23. Trifari, S., C. D. Kaplan, E. H. Tran, N. K. Crellin, and H. Spits. 2009. Identification of a human helper T cell population that has abundant production of interleukin 22 and is distinct from T_H-17, T_H1 and T_H2 cells. *Nat. Immunol.* 10: 864–871.
24. Basu, R., D. B. O'Quinn, D. J. Silberger, T. R. Schoeb, L. Fouser, W. Ouyang, R. D. Hatton, and C. T. Weaver. 2012. Th22 cells are an important source of IL-22 for host protection against enteropathogenic bacteria. *Immunity* 37: 1061–1075.
25. Spits, H., and T. Cupedo. 2012. Innate lymphoid cells: emerging insights in development, lineage relationships, and function. *Annu. Rev. Immunol.* 30: 647–675.
26. Walker, J. A., J. L. Barlow, and A. N. McKenzie. 2013. Innate lymphoid cells—how did we miss them? *Nat. Rev. Immunol.* 13: 75–87.
27. Hori, T., H. Ohnishi, T. Teramoto, K. Tsubouchi, T. Naiki, Y. Hirose, O. Ohara, M. Seishima, H. Kaneko, T. Fukao, and N. Kondo. 2012. Autosomal-dominant chronic mucocutaneous candidiasis with STAT1-mutation can be complicated with chronic active hepatitis and hypothyroidism. *J. Clin. Immunol.* 32: 1213–1220.

nature COMMUNICATIONS

ARTICLE

Received 10 Jul 2014 | Accepted 20 Sep 2014 | Published 15 Dec 2014

DOI: 10.1038/ncomms6340 OPEN

The structural basis for receptor recognition of human interleukin-18

Naotaka Tsutsumi[1,*], Takeshi Kimura[2,*], Kyohei Arita[3], Mariko Ariyoshi[1,4], Hidenori Ohnishi[2], Takahiro Yamamoto[2], Xiaobing Zuo[5], Katsumi Maenaka[6], Enoch Y. Park[7], Naomi Kondo[2,8], Masahiro Shirakawa[1,9], Hidehito Tochio[10] & Zenichiro Kato[2,11]

Interleukin (IL)-18 is a proinflammatory cytokine that belongs to the IL-1 family and plays an important role in inflammation. The uncontrolled release of this cytokine is associated with severe chronic inflammatory disease. IL-18 forms a signalling complex with the IL-18 receptor α (Rα) and β (Rβ) chains at the plasma membrane, which induces multiple inflammatory cytokines. Here, we present a crystal structure of human IL-18 bound to the two receptor extracellular domains. Generally, the receptors' recognition mode for IL-18 is similar to IL-1β; however, certain notable differences were observed. The architecture of the IL-18 receptor second domain (D2) is unique among the other IL-1R family members, which presumably distinguishes them from the IL-1 receptors that exhibit a more promiscuous ligand recognition mode. The structures and associated biochemical and cellular data should aid in developing novel drugs to neutralize IL-18 activity.

[1] Department of Molecular Engineering, Graduate School of Engineering, Kyoto University, Katsura, Nishikyo-ku, Kyoto 615-8510, Japan. [2] Department of Pediatrics, Graduate School of Medicine, Gifu University, Yanagido 1-1, Gifu 501-1194, Japan. [3] Graduate School of Nanobioscience, Yokohama City University, 1-7-29 Suehiro-cho, Tsurumi-ku, Yokohama Kanagawa 230-0045, Japan. [4] Institute for Integrated Cell-Material Sciences, Kyoto University, Kyoto 606-8501, Japan. [5] X-Ray Science Division, Argonne National Laboratory, 9700 South Cass Avenue, Argonne, Illinois 60439, USA. [6] Laboratory of Biomolecular Science and Center for Research and Education on Drug Discovery, Faculty of Pharmaceutical Sciences, Hokkaido University, , Kita-12, Nishi-6, Kita-ki, Sapporo 060-0812, Japan. [7] Research Institute of Green Science and Technology, Department of Bioscience, Graduate school of Science and Technology, Shizuoka University, 836 Ohya Suruga-ku, Shizuoka 422-8529, Japan. [8] Heisei College of Health Sciences, 180 Kurono, Gifu 501-1131, Japan. [9] Core Research of Evolution Science (CREST), Japan Sciences and Technology Agency, Tokyo 102-0076, Japan. [10] Department of Biophysics, Graduate School of Science, Kyoto University, Kitashirakawa-oiwake, Sakyo-ku, Kyoto 606-8502, Japan. [11] Biomedical Informatics, Medical Information Sciences Division, The United Graduate School of Drug Discovery and Medical Information Sciences, Gifu University, Gifu 501-1194, Japan. * These authors contributed equally to this work. Correspondence and requests for materials should be addressed to H.O. (email: ohnishih@gifu-u.ac.jp) or to H.T. (email: tochio@mb.biophys.kyoto-u.ac.jp).

Interleukin (IL)-18 belongs to the IL-1 superfamily and was first discovered as an interferon gamma (IFN-γ)-inducing factor in sera from mice with hepatitis stimulated with *Propionibacterium* acnes and lipopolysaccharide[1]. This proinflammatory cytokine is secreted by various types of cells and strongly augments IFN-γ production in type-1 helper T (Th1) cells and natural killer (NK) cells following activation of NK-cell cytotoxicity; thus, it plays a critical role in inflammation and the host defense against microbes. In addition to IL-1β[2,3], IL-18 is synthesized as a biologically inactive precursor (proIL-18) on activation of a certain class of receptors, such as Toll-like receptors and proinflammatory cytokine receptors, and then stored in the cytosol. Once it matures via caspase-1 (ref. 4), which is regulated by a large protein complex referred to as the inflammasome[5], IL-18 is extracellularly secreted and binds IL-18 receptor α (Rα) as well as IL-18 receptor β (Rβ) at the immunocyte plasma membrane in a stepwise manner. IL-18/IL-18Rα/IL-18Rβ ternary complex formation juxtaposes the intracellular Toll-Interleukin-1 receptor domains of IL-18Rα and IL-18Rβ, to which the adaptor molecule myeloid differentiation factor 88 (MyD88) is recruited presumably with the aid of TRAM[6]. MyD88 further interacts with IL-1 receptor associating kinase (IRAK) 4 and IRAK1/2 to form the large molecular assembly referred to as Myddosome, which subsequently activates IKK via TRAF6. Finally, the signal activates the NF-κB and mitogen-activated protein kinase pathways[7], which upregulate the expression of various inflammatory cytokines.

Of the IL-1 family cytokines, IL-18 and IL-1β have garnered much attention because they are causal cytokines that lead to severe chronic inflammatory syndrome. IL-1β is associated with immunological disorders, such as autoinflammatory syndromes[8,9]. The central pathogenic feature of autoinflammatory syndromes is excess production of mature IL-1β derived from abnormal inflammasome activation due to certain gene mutations. IL-1β-related autoinflammatory diseases are treated through neutralizing IL-1β by anti-IL-1β (canakinumab and gevokizumab), engineered soluble receptors (rilonacept) or the receptor antagonist IL-1Ra (anakinra), which is remarkably effective; thus, these treatments are currently in clinical use[10]. Similar to IL-1β, IL-18 overproduction likely leads to severe autoimmune, autoinflammatory, allergic, neurological and metabolic disease, which might be associated with IL-18 or IL-18 receptor genetic polymorphisms[11–14]. Two recent papers have revealed that constitutive activation of the inflammasome caused by single point mutations in NLRC4 is associated with a novel autoinflammatory disorder, and the patient with NLRC4-mediated macrophage activation syndrome showed ultra-high circulation levels of IL-18 even after IL-1 blockade[15,16]. Consistent with these observations, therapeutic approaches that block IL-18 activity have been effective in inflammatory disease models[17,18]. Therefore, developing drugs that impede binding between IL-18 and the receptors is clinically important. Generally, the atomic structures of targeted proteins and their complexes play vital roles in drug design. Thus far, despite the reported structures for free IL-18 and its related complexes[19–22], a structure for the genuine complex between IL-18 and its receptors has not yet been determined.

Previously, we reported a solution structure for IL-18 and identified the functional residues for which mutation markedly decreased its binding affinity for IL-18Rα[19]. The results suggest that the binary complex between IL-18 and IL-18Rα exhibits an essentially identical binding mode to the complex between IL-1β and its receptors (IL-1RI or IL-1RII). However, the binding mode for IL-18Rβ, which is the IL-18 co-receptor, to IL-18/IL-18Rα remained ambiguous. Recent structural studies on the ternary complex between IL-1β and its receptors' ectodomains[23,24] demonstrate that IL-1RAcP, which is the commonly used co-receptor for IL-1α, IL-1β, IL-33 and IL-36s, adopted a 'left' binding mode. In this mode, IL-1RAcP binds the IL-1β/IL-1RI or IL-1β/IL-1RII binary complexes from the left side as seen from the concave IL-1β recognition surface of IL-1RI or IL-1RII. Furthermore, the other IL-1 superfamily molecule, IL-33/ST2/IL-1RAcP, was also suggested to adopt the 'left' binding mode based on the model structure from the small angle X-ray scattering (SAXS) profiles[25]. Thus, left binding seems common in complexes that employ IL-1RAcP. In contrast to other IL-1 family cytokines, IL-18 is unique due to its pair of specialized receptors (IL-18Rα and IL-18Rβ); hence, the recognition details are not sufficiently understood based only on homology to the IL-1β and IL-33 system.

Here, we performed X-ray crystallography using human IL-18 and its complexes with the receptors' extracellular domains. The structures demonstrate that the co-receptor (IL-18Rβ) binding mode is generally identical to IL-1β; however, substantial differences were observed in the subdomain orientations and interaction details throughout the complex. Intriguingly, the second domain (D2) of the two IL-18 receptors lacked one β-strand, d2, which is conserved among other IL-1-related receptors, and was previously shown to contribute to the inter-receptor interaction. In addition, N-linked glycans played a role in bridging the two receptors, which was observed in the signalling IL-1β receptor complex but was absent in its decoy complex. We further show that other IL-18Rα N-linked glycans proximal to IL-18 in the complexes contributed to the binding affinity. With the associated biochemical and cell biological data, the structures comprehensively clarify the IL-18 receptor recognition mode, which will facilitate rational drug development to neutralize IL-18 activity, the uncontrolled release of which has been shown to cause severe chronic inflammatory diseases.

Results

Structural comparison between the IL-18 and IL-1β complexes. We determined the crystal structures of IL-18 (Fig. 1a), the IL-18/IL-18Rα binary complex (Fig. 1b) and the IL-18/IL-18Rα/IL-18Rβ signalling ternary complex (Fig. 1c,d) at the resolutions 2.33, 3.10 and 3.10 Å, respectively. The crystallographic statistics are provided in Table 1.

IL-18Rα curls around IL-18, and IL-18Rβ contacts the lateral portion of the IL-18/IL-18Rα binary complex in a similar manner as the IL-1β/IL-1RI(RII)/IL-1RAcP complex[23,24]. The IL-18 structure essentially does not change on complex formation, maintaining the β-trefoil fold that comprises 12 β-strands (β1-β12) and 2 α-helices (α1-α2) (Supplementary Fig. 1a), as previously reported[19]. The IL-18Rα ectodomain folds into three immunoglobulin (Ig)-like domains, which are referred to as D1, D2 and D3, in the same manner as the IL-1 receptors[23,24,26]. Each domain comprises a two-layer sandwich of six to nine β-strands and contains at least one intra-domain disulfide bond (Supplementary Fig. 1b). Within IL-18Rα, D1 extensively contacts D2, whereas D3 is distant and is connected by the long D2-D3 linker (Fig. 1d middle), which implies that D1 and D2 behave as a single module, similar to IL-1-related primary receptors. In the Ig superfamily, including the IL-1 receptor family (Fig. 2a), the core cysteine residues on the b and f strands are highly conserved (Fig. 2b). However, for IL-18Rα-D1, the f strand cysteine is replaced with phenylalanine (Fig. 2b), which yields two unexpected surface disulfide bonds (Fig. 2c). In addition, the D2 domain lacks one β-strand (d2 in Fig. 2b,d) that is structurally conserved among most IL-1 receptor family members, IL-1RI, IL-1RII and ST2 as well as IL-1RAcP.

On ternary complex formation, the IL-18/IL-18Rα binary complex structure essentially does not change; the root mean

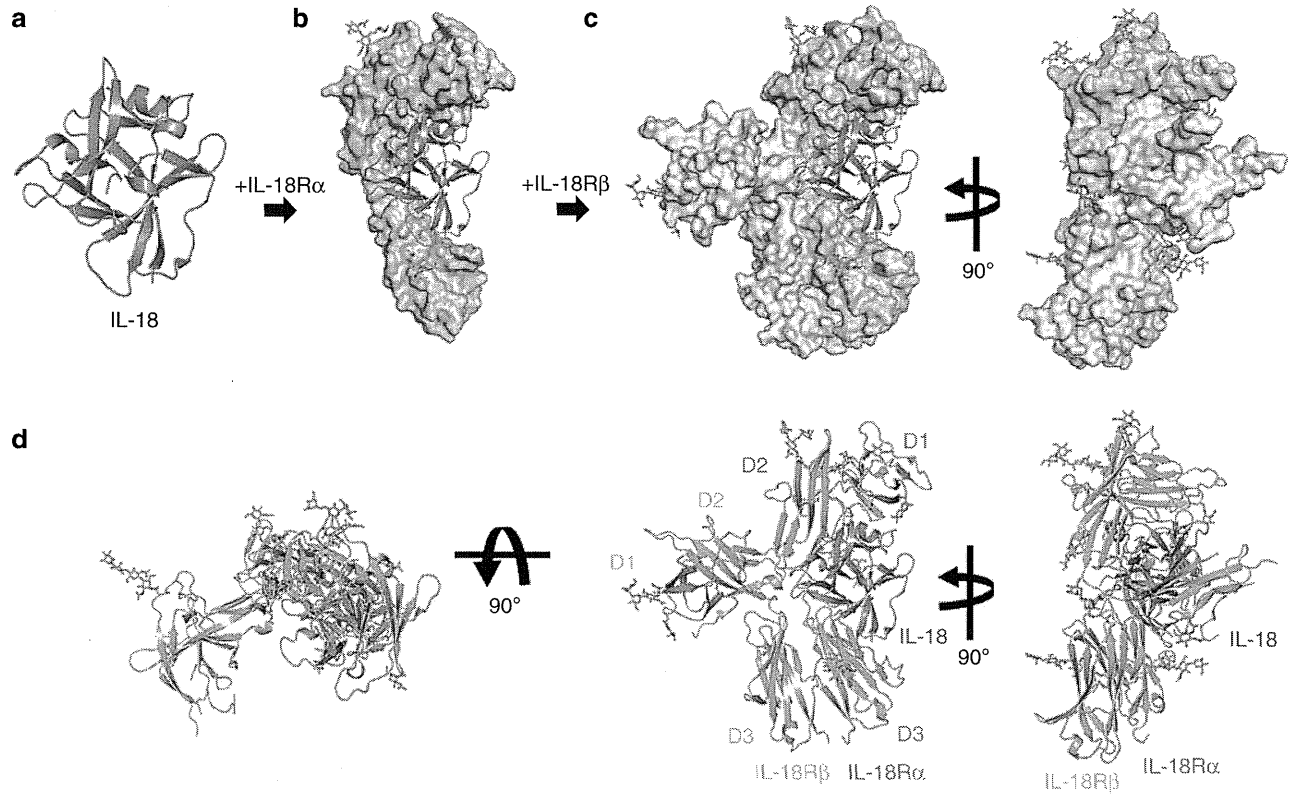

Figure 1 | Overall structures for IL-18 and its extracellular complexes. (**a**–**c**) Schematic flow diagram of the stepwise complex formation for IL-18/IL-18Rα/IL-18Rβ. Crystal structures of (**a**) IL-18, (**b**) IL-18/IL-18Rα and (**c**) IL-18/IL-18Rα/IL-18Rβ are shown as a ribbon (IL-18, blue) or surface (IL-18Rα, palegreen; IL-18Rβ, wheat) representation, respectively. (**d**) Ribbon diagrams of the ternary complex structure for IL-18 (blue), IL-18Rα (green) and IL-18Rβ (orange) from three perspectives.

square deviations (RMSD) for the backbone Cα atoms are 0.41–0.90 Å compared with the asymmetric unit (ASU) molecules. IL-18Rβ is also composed of three Ig-like domains, similar to IL-18Rα except for the aforementioned disulfide bonds (Supplementary Fig. 1c); however, the spatial arrangement of these domains is markedly distinct from IL-18Rα in the ternary complex (Fig. 1d). D2 and D3 of IL-18Rβ are close to each other and directly associated with IL-18/IL-18Rα, while D1 does not contribute to ternary complex formation. In fact, a part of the IL-18Rβ-D1 electron density is ambiguous presumably because the region was loosely packed in the crystal (Supplementary Fig. 2). The D1 isolation of the co-receptor was also observed previously in the IL-1β/IL-1RI(RII)/IL-1RAcP complex, where IL-1RAcP-D1 is outstretched and does not participate in the molecular interface. Despite of the similarity in the binding mode, relative orientation of IL-18Rβ-D2 + D3 to IL-18/IL-18Rα is different from that of IL-1RAcP-D2 + D3 to IL-1β/IL-1RI(RII) (Fig. 3a–c). This difference in the orientations is attributable to the interaction manner at the interface between IL-18Rβ-D2 and IL-18/IL-18Rα (Fig. 3b,d). Owing to the aforementioned absence of the d2 strands in D2s (Fig. 2b,d), IL-18Rα-D2 and IL-18Rβ-D2 supply only two strands (b2 and e2) and loops at the interface, respectively, while for IL-1RI(RII) and IL-1RAcP-D2, three strands (b2, e2 and d2) and loops interact (Fig. 1d and Fig. 3a–c). Furthermore, IL-18Rβ-D2 supplies not only electrostatic side chains but also aromatic rings that interact with IL-18, whereas IL-1RAcP-D2 utilizes electrostatic and aliphatic side chains for ligand binding. The β4-β5 loop of IL-18 and IL-18Rβ-D3 do not interact, which may also contribute to the orientation difference (Fig. 3d). A more marked dissimilarity is observed for the IL-18Rβ-D1 orientation relative to -D2, which differs from IL-1RAcP in the complex (Fig. 3e). As a result, despite the same 'left' binding mode, the spatial arrangements of the subdomains in the IL-18/IL-18Rα/IL-18Rβ ternary complex differ somewhat from IL-1β/IL-1RI/IL-1RAcP with Cα atom RMSD values of 6.64–6.73 Å.

The binding interface between IL-18 and IL-18Rα. IL-18Rα recognizes IL-18 through a large interaction surface area at ~1,850 Å^2. Two IL-18 sites, Sites I and II, contact IL-18Rα; Site I is located on a side of the core barrel of the β-trefoil structure, and Site II is at the top of the β-barrel (Fig. 4a).

Our previous NMR study showed that the residues 34 to 42 are flexible despite partial α-helix formation in this region (residues 38–41)[19]. In addition, two isomeric forms that originate from a *cis* or *trans* peptide bond between Ala42$^{IL\text{-}18}$-Pro43$^{IL\text{-}18}$ in the loop are equally populated in the solution structure. The flexible nature of the segment produces a variety of architectures, as demonstrated in several crystallographic reports, including a loop with a *trans* isomer[22], an α-helix with a *cis* isomer[21] or, primarily, unobservable flexible loop with a *trans* isomer[20,22] (Fig. 4a–c). In both the binary and ternary complexes, the segment between residues 35 and 40 adopts an α-helix structure with a *cis* Ala42$^{IL\text{-}18}$-Pro43$^{IL\text{-}18}$ bond, which is stabilized by hydrogen bonds and electrostatic interactions with IL-18Rα (Fig. 4c).

Surrounding Site I, α-helix I mediated the interaction (Fig. 4c and Fig. 5a), wherein the Arg25$^{R\alpha}$ side chain is buried within the β3-α1 acidic groove of IL-18. Two disulfide bonds, Cys22$^{R\alpha}$-Cys41$^{R\alpha}$ and Cys43$^{R\alpha}$-Cys81$^{R\alpha}$, bridge the b1-c1 loop to the N-terminal loop and d1-e1 turn, respectively (Figs 2c and 5a), which likely reinforce the proximal loop structure, to which the long β10-β11 hairpin of IL-18 is fitted. This unique feature

Table 1 | X-ray crystallographic statistics of IL-18 and its extracellular complexes.

	IL-18	IL-18/IL-18Rα	IL-18/IL-18Rα/IL-18Rβ
Data collection			
Beamline	BL38B1 (SPring-8)	BL44XU (SPring-8)	BL17A (Photon Factory)
Wavelength	1.0000	0.9000	0.9800
Space group	$P2_1$	$P2_12_12$	$P2_12_12_1$
Cell dimensions			
a, *b*, *c* (Å)	68.15, 79.51, 73.46	135.49, 174.81, 183.40	72.56, 111.56, 134.57
α, β, γ (°)	90.00, 100.97, 90.00	90.00, 90.00, 90.00	90.00, 90.00, 90.00
Resolution (Å)	45.0-2.33 (2.46-2.33)	43.9-3.10 (3.27-3.10)	50.0-3.10 (3.21-3.10)
R_{merge}	4.9 (39.6)	10.0 (58.2)	11.5 (68.3)
$I/\sigma I$	20.5 (3.6)	14.9 (2.5)	19.8 (2.9)
Completeness (%)	97.8 (97.1)	99.6 (100)	99.9 (99.3)
Redundancy	3.8 (3.8)	3.7 (3.8)	9.8 (9.2)
Refinement			
Resolution (Å)	34.82-2.33 (2.41-2.33)	42.00-3.10 (3.18-3.10)	42.00-3.10 (3.29-3.10)
No. reflections	32,157 (2,861)	79,130 (5,821)	17,368 (1,825)
R_{work}/R_{free}	21.8/27.1 (27.6/29.8)	19.1/22.2 (22.7/26.3)	18.8/23.2 (20.9/29.7)
No. atoms			
Protein	5,022	20,533	5,663
Glycan	—	1,225	335
Others	711	289	32
B-factors			
Protein	46.13	78.31	74.38
Glycan	—	121.43	139.74
Others	60.94	109.02	36.55
R.m.s. deviations			
Bond lengths (Å)	0.010	0.009	0.009
Bond angles (°)	1.38	1.11	1.17
Ramachandran plot	95.2, 4.8	94.4, 5.0, 0.5	93.7, 5.4, 0.8

Values for Ramachandran plots are presented as favoured, allowed, outlier examined by RAMPAGE. Data collection statistics were summarized from the report[35].

implies that the loop structure may be loosened under certain reductive conditions, which affects the affinity for the ligand. The Ser42$^{R\alpha}$ amide proton supplies a hydrogen bond for the Asp132$^{IL\text{-}18}$ side chain, which also exhibited a backbone–backbone hydrogen bond with Cys22$^{R\alpha}$. Around Site II (Fig. 5b), the IL-18Rα acidic surface, which is composed of the Glu253$^{R\alpha}$ and Glu263$^{R\alpha}$ carboxylates as well as Trp249$^{R\alpha}$ backbone oxygen, captures the Lys53$^{IL\text{-}18}$ ε-amino group.

IL-18Rβ recognition by IL-18/IL-18Rα. The IL-18/IL-18Rα/IL-18Rβ signalling ternary complex is formed by IL-18Rβ binding with the lateral portion of the binary complex (Fig. 1). The IL-18Rβ-D2 convex surface with the key Tyr212$^{R\beta}$ aromatic residue fits into the concave surface jointly formed by IL-18 and IL-18Rα-D2 (Fig. 5c and Supplementary Fig. 3a) with a 613 Å^2 buried surface area, which is shallower than that in the IL-1β complexes. The concave surface area is divided into Site III on IL-18 (354 Å^2, Fig. 5c) and part of IL-18Rα-D2 (259 Å^2, Supplementary Fig. 3a). Note that IL-18 Site III is revised in this work[19]. Site III of IL-18 comprises the prominent β8-β9 hairpin and β11-α2 loop (Fig. 5c), where the aromatic ring of His109$^{IL\text{-}18}$ forms π-π stacking with Tyr212$^{R\beta}$ at a 3.4 Å distance, which is surrounded and stabilized by multiple hydrogen bonds. IL-18Rα-D2 is composed of an antiparallel β-sheet formed by b2 and e2 (Supplementary Fig. 3a) but lacks the conserved d2 strand compared with the corresponding β-sheets of IL-1RI and ST2. Although the structure of IL-36R has not been determined yet, the multiple sequence alignment suggests that the b2/e2/d2 sheet is conserved among the primary receptors (Fig. 1b and Supplementary Fig. 1b). In addition to these interactions, IL-18Rβ-D3 extensively contacts IL-18Rα-D3 with the buried area ~550 Å^2, to which both electrostatic (Supplementary Fig. 3b) and hydrophobic interactions (Supplementary Fig. 3c) contribute. These inter-receptor interfaces in the IL-1β complex are designated as Site IV[23], in which the IL-1β β4-β5 loop interacts with IL-1R1-D3 and IL-1RAcP-D3 to at least partly establish the ligand's agonism/antagonism. The same would be true for the IL-36 system based on the crystal structure of IL-36 (ref. 27). In contrast, the corresponding IL-18 loop does not contact IL-18Rβ-D3 and only interacts with IL-18Rα-D3 (Fig. 3d).

N-linked IL-18Rα glycans and its interactions. In the IL-18/IL-18Rα and IL-18/IL-18Rα/IL-18Rβ crystal structures, seven N-linked glycosyl chains were identified in IL-18Rα at Asn91, 102, 150, 197, 203, 236 and 297 (Fig. 6a). These carbohydrates are high-mannose glycans (Fig. 6b) because the receptor proteins were prepared using the Sf9 expression system. The glycan on Asn197$^{R\alpha}$, which are located in the D2 domain, forms moderate intramolecular interactions with Arg114$^{R\alpha}$ and His117$^{R\alpha}$ at the D1-D2 loop (Fig. 6c), seemingly contributing to the subdomains' spatial arrangement. The core-NAG (N-acetyl-D-glucosamine) directly linked to Asn297$^{R\alpha}$ branches into the second-NAG and L-fucose (FUC), which is referred to as the core-FUC (Fig. 6b–d). Interestingly, the core-FUC and second-NAG on Asn297$^{R\alpha}$ are proximal to the β4-β5 loop of IL-18 (<4 Å); hence, they likely interact through electrostatic and hydrophobic interactions with the ligand (Fig. 6d) and partly contribute the unique D3:D3 interaction.

Notably, the NAG-NAG extended from the IL-18Rα-D3 Asn236$^{R\alpha}$ and points to the receptor C-terminus in the binary complex; however, in the ternary complex, the NAG-NAG chain changes direction and points to IL-18Rβ-D3 within the distance possibly to form electrostatic interaction with Val257$^{R\beta}$ and Asp259$^{R\beta}$ (Fig. 6e). A similar inter-receptor interaction via an

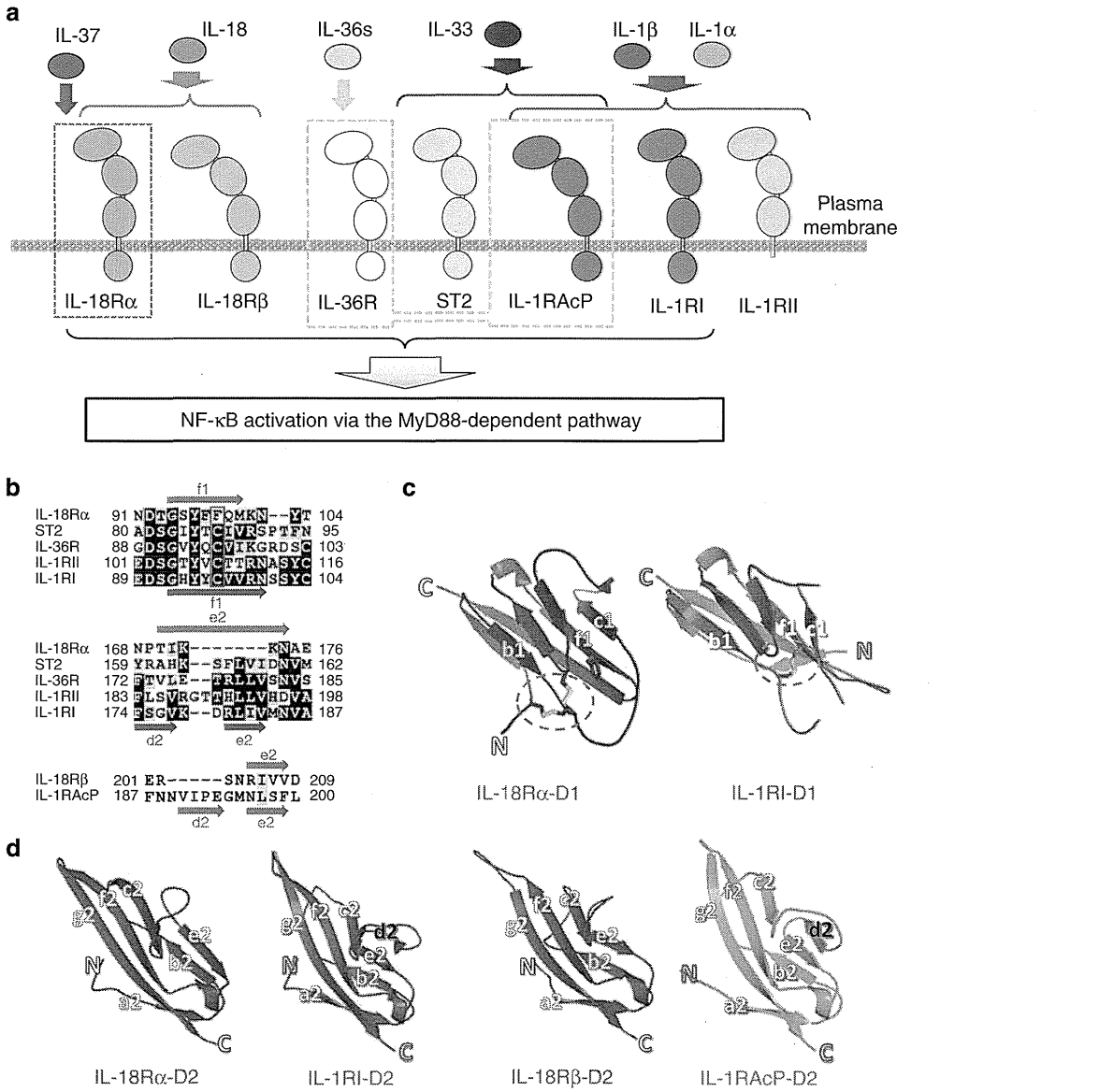

Figure 2 | Structural features of IL-18 and its receptors. (**a**) Promiscuous interactions between the IL-1 family agonists and IL-37 with the receptor molecules. Except IL-18, all agonists employ IL-1RAcP as a co-receptor, while IL-18 uses IL-18Rβ. (**b**) Certain regions of the receptor multiple sequence alignments manifest the unique qualities of IL-1R family IL-18Rs. The full set of sequence alignments is in Supplementary Fig. 1. (**c**) Structural comparison of D1 and (**d**) D2 of the receptors from the signalling complex. The green circles in (**c**) show the disulfide bond positions.

N-linked oligosaccharide was previously observed between IL-1RI-D3 and IL-1RAcP-D3 in the IL-1β signalling complex, but it is intriguingly absent in the IL-1β/IL-1RII/IL-1RAcP non-signalling decoy complex, which suggests that the N-linked oligosaccharides bridging the two receptors are important for IL-1 family signal transduction.

Characterization of IL-18/IL-18Rα/IL-18Rβ in solution. A previous SPR analysis showed that IL-18Rβ does not bind free IL-18, but it does bind a preformed IL-18/IL-18Rα binary complex[19]. To better understand the formation of this complex under more physiological conditions, we performed titration experiments using solution NMR spectroscopy. The ^{1}H–^{15}N correlation spectrum for [^{2}H,^{15}N]-IL-18 did not change on adding a small excess of IL-18Rβ, indicating that the molecules do not interact. However, marked spectral changes were observed when IL-18 was titrated with IL-18Rα (Supplementary Fig. 4a,b). The amino-acid residues that were perturbed during the titration are at the molecular interface of the binary complex, which indicates that the binding mode in solution is identical to the crystal structure (Supplementary Fig. 4b, bottom). Cross-saturation NMR experiments[28] further confirmed this result with more precision (Fig. 7a, forest and Supplementary Fig. 4c). Next, IL-18Rβ was added to the preformed [^{2}H,^{15}N]-IL-18/IL-18Rα binary complex. The ^{1}H–^{15}N correlation spectrum was then changed due to ternary complex formation. Although significant changes were not observed in the region including the previously defined Site III (Supplementary Fig. 4d), the cross-peaks that disappeared or shifted on ternary complex formation (Supplementary Fig. 4e) are mostly at the interface with IL-18Rβ, which is consistent with the ternary complex crystal structure (Fig. 7a, orange). Furthermore, we performed SAXS to analyse the architecture of the ternary complex (Supplementary Fig. 4f–h); these data were used to construct a low-resolution dummy atom model. The crystal structure of the complex reasonably fits the SAXS-derived model envelope (Fig. 7b). Together, the crystal

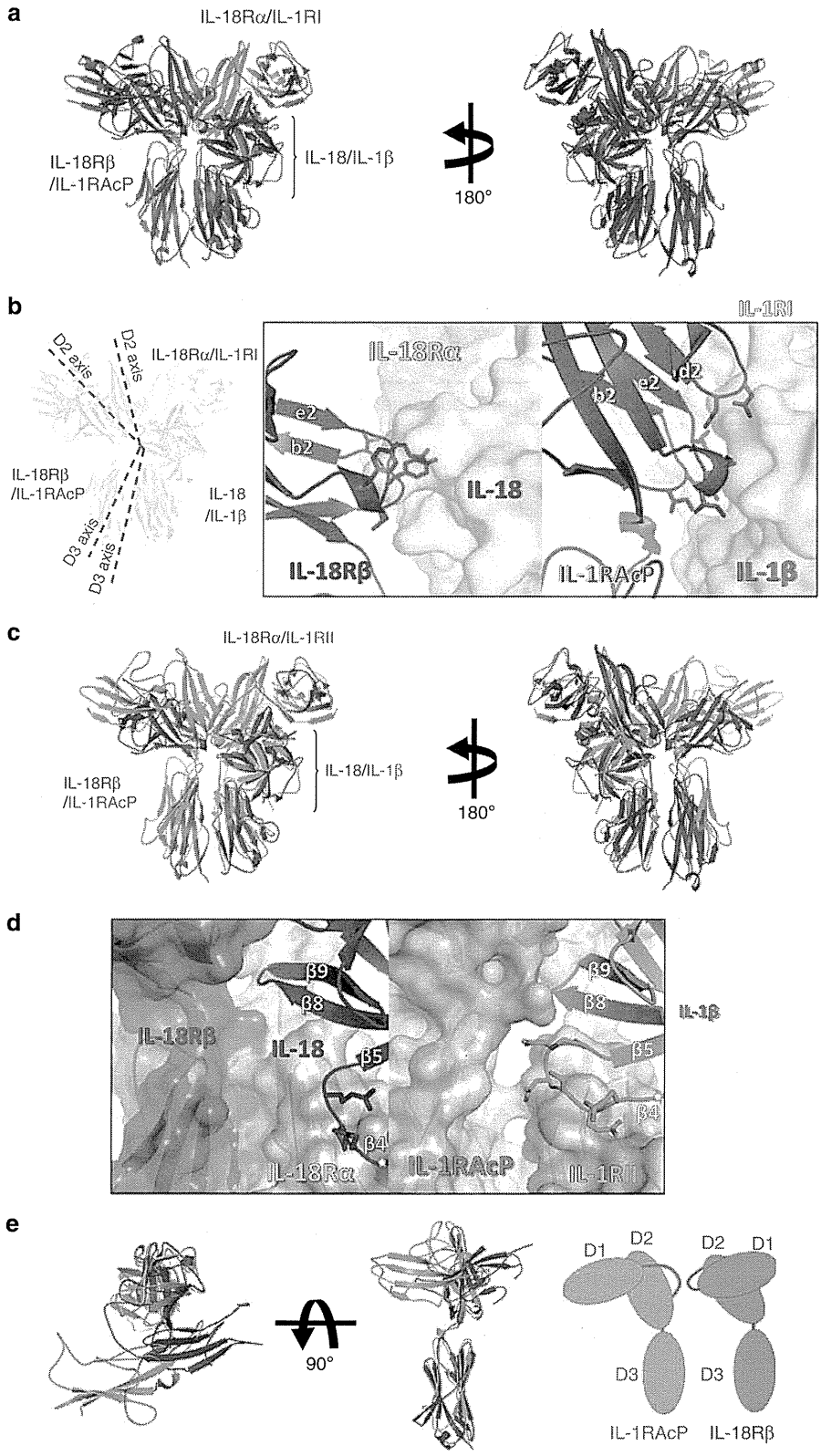

Figure 3 | Structural comparison of the IL-1 family cytokine ternary complexes. (**a**) Structural alignment of IL-18/IL-18Rα/IL-18Rβ (blue) and IL-1β/IL-1RI/IL-1RAcP (4DEP, red) using the binary complex region. The backbone Cα RMSD between IL-18/IL-18Rα and IL-1β/IL-1RI is 4.35–4.36 Å. (**b**) The orientation of D2 and D3 from IL-18Rβ and IL-1RAcP in the complexes. The dotted lines show the approximate orientation of the longitudinal D2 and D3 axes. A close-up of the binary complex interface, which recognizes the co-receptor protein D2 domains, is also shown. (**c**) A comparison of IL-18/IL-18Rα/IL-18Rβ (blue) and IL-1β/IL-1RII/IL-1RAcP (3O4O, green). The backbone Cα RMSD was 4.39 Å surrounding the binary complex portion. (**d**) A close-up of the β4-β5 loops of the ligands in IL-18/IL-18Rα/IL-18Rβ (left) and IL-1β/IL-1RII/IL-1RAcP (right). (**e**) Superimposition of IL-18Rβ and IL-1RAcP (from 3O4O). The IL-18Rβ-D1 orientation relative to D2 is the opposite of IL-1RAcP.

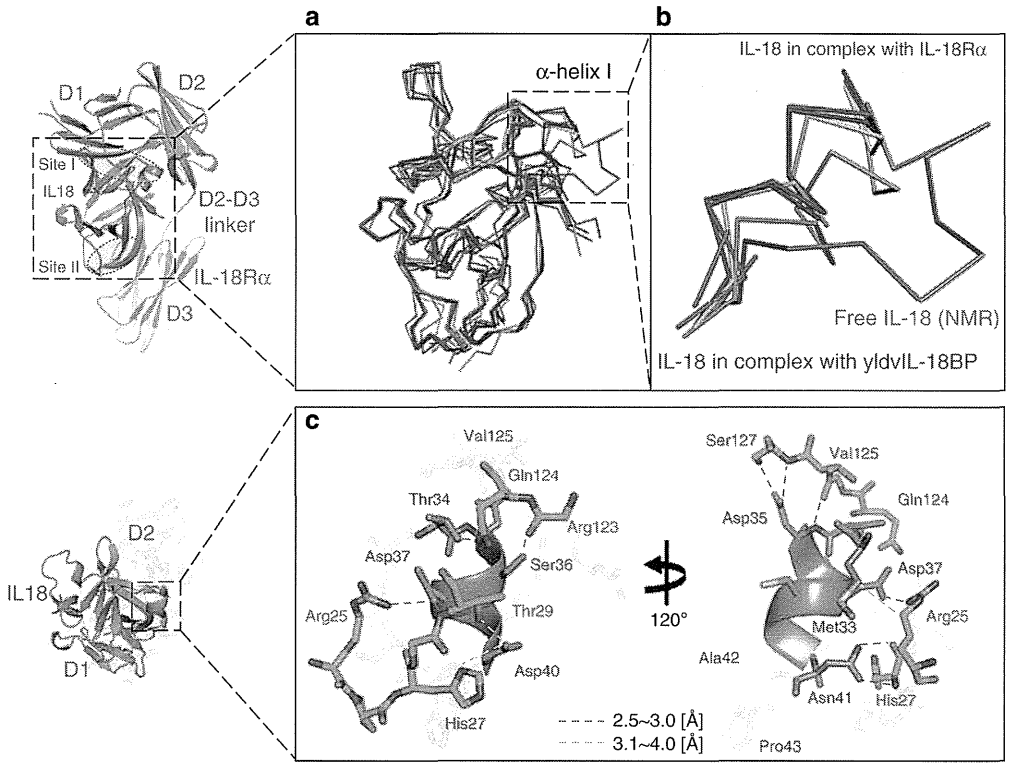

Figure 4 | IL-18 structural perturbations on binding IL-18Rα or other proteins. (**a**) Superimposition of the structures of IL-18 in free and various complex forms: crystal structure of IL-18 with CHPAS (red); the solution structure (1J0S, raspberry); the crystal structure of IL-18 in complex with Ectromelia virus IL-18BP (3F62, pink); the crystal structure of IL-18 complexed with murine reference antibody 125-2H Fab (2VXT, salmon); the crystal structure for IL-18 in complex with YLDV 14L IL-18BP (4EEE, brown); the crystal structure for IL-18 in complex with a DVD-Ig molecule (4HJJ, gray); the crystal structure of IL-18 in complex with IL-18Rα (blue). (**b**) The zoom window of the dashed line box shown in 2**a**. (**c**) The stabilized structure and IL-18 α-helix I interactions. The structure of IL-18 α-helix I stabilized by interactions with IL-18Rα.

structures solved in this study are consistent with the data collected in the solution state, which underscores the physiological significance of the crystal structures.

Effects of mutation on the signaling and binding affinities. To confirm the importance of the IL-18 Site III interactions in signal transduction, we performed cell-based assays using IL-18Rβ mutants (Fig. 8a). IL-18Rβ-WT and its mutants were transiently expressed in HEK293 cells with a background of stably expressed IL-18Rα; the NF-κB activity was measured using the luciferase reporter system with or without an IL-18 stimulus. A complete loss of function was observed for the IL-18Rβ-E210A-Y212A-Y214A triple mutants, while IL-18Rβ-E210A, -Y212A and -K313A exhibited approximately half the activity compared with -WT. Remarkably, only a minor decrease in activity was observed when the D1 region of IL-18Rβ was deleted (Δ15–65 and Δ15–146, Fig. 8b), likely because IL-18Rβ-D1 is distal to the other parts of the ternary complex and seemingly does not affect binding. However, a substantial decrease in activity was observed when the D1-D2 loop (Δ15–153) was deleted, and the activity was fully abolished in the D1/D2-deficient experiments (Δ15–176 and Δ15–243). Therefore, IL-18Rβ-D2 + D3 is sufficient, but D1 is not essential for signalling.

To identify the amino-acid residues that are critical for ternary complex formation, we performed a binding study using surface plasmon resonance (SPR) analysis (Supplementary Figs 5 and 6 and Supplementary Table 1). The prominent binding residues are summarized in Table 2 and Supplementary Fig. 7. First, IL-18Rβ was immobilized on the sensor chip, and binary complexes that formed between one of IL-18 mutants and IL-18Rα were examined for binding. When the binary complex contained either of three IL-18 mutants, G108A, H109A or K112A, it lost affinity for IL-18Rβ, even though these mutants maintained full binding activity for IL-18Rα. Thus, the mutated residues are only important for IL-18Rβ binding. Next, one of IL-18Rβ mutants was immobilized on the sensor chip, and the IL-18/IL-18Rα binary complex was examined for binding. Our data show that IL-18Rβ-Y212A did not bind the binary complex, which is consistent with the structure, wherein substantial π-π stacking were observed between $Tyr212^{R\beta}$ and $His109^{IL\text{-}18}$ (Fig. 5c). IL-18Rβ-K313A and -E210A exhibited 7- and 20-fold lower affinity for the IL-18/IL-18Rα complex relative to the wild-type receptor, respectively. These data are also consistent with the NF-κB luciferase reporter assay and the structure, wherein the mutated residues extensively interact with $His109^{IL\text{-}18}$, $Asp110^{IL\text{-}18}$, $Lys112^{IL\text{-}18}$ and $Phe135^{R\alpha}$ (Fig. 5c and Supplementary Fig. 3a).

To determine the contribution of the IL-18Rα N-linked oligosaccharides to the receptor complex formation, we mutated two IL-18Rα asparagine residues to glutamine (Table 2). The affinity of IL-18 for IL-18Rα decreased to one-third when $Asn297^{R\alpha}$ was mutated to Gln compared with the wild type, which indicates that the sugar chain is important for the recognition of ligand, wherein the $Asn297^{R\alpha}$ core-FUC and second-NAG are proximal to IL-18 (Fig. 6d). However, we did not observe a different affinity on mutating $Asn236^{R\alpha}$.

Discussion

It is well-known that the IL-1 family system has only two co-receptors, IL-1RAcP and IL-18Rβ, despite its seven agonists (IL-1α, IL-1β, IL-18, IL-33, IL-36α, IL-36β and IL-36γ) and four

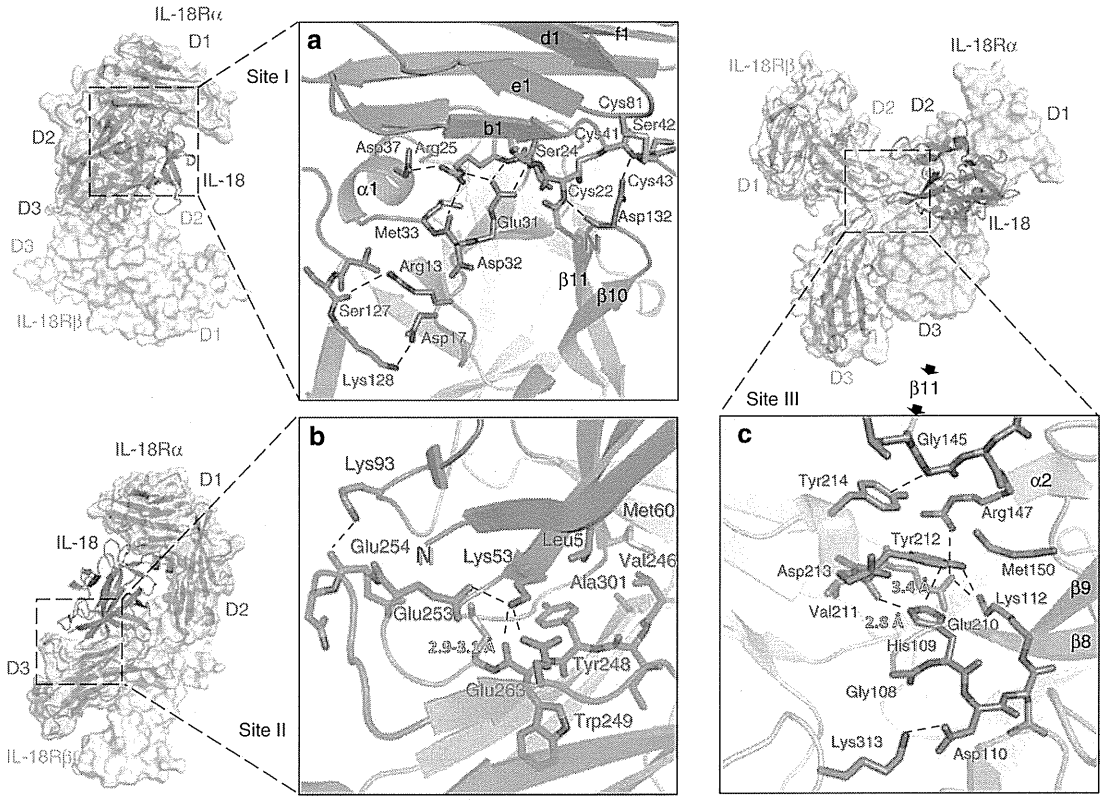

Figure 5 | The key residues involved in forming the ternary signalling complex. (**a**) The interactions in the IL-18 receptor binding Site I. In addition to the area surrounding the stable α-helix I, Asp132^{IL-18} at the tip of the β10-β11 hairpin exhibits ionic interactions with the structure, which are formed by the two unique disulfide bonds in IL-18Rα. (**b**) Interactions surrounding the IL-18 Site II. The key residue of Lys53^{IL-18} is recognized by the IL-18Rα acidic surface through multiple hydrogen bonds. (**c**) The interface between Site III of IL-18 and IL-18Rβ. In addition to His109^{IL-18}/Tyr212^{Rβ} stacking, multiple hydrogen bonds were observed: the His109^{IL-18} Nε-H to the Val211^{Rβ} backbone carbonyl oxygen as well as the Lys112^{IL-18} Nζ-H to the Glu210^{Rβ} side chain and Tyr212^{Rβ} Oη.

primary receptors (IL-1RI, IL-18Rα, ST2 and IL-36R)[29]. Thus, certain receptors must be used by multiple ligands (Fig. 2a). In fact, IL-1RAcP is commonly involved in signals with six ligands other than IL-18, which is recognized by its specific receptors, IL-18Rα and IL-18Rβ. Accordingly, the IL-18 binding mode remained unclear even after several crystal structures of the IL-1β and receptor complexes became available. The IL-18 complex structures determined in this work exhibited essentially the same binding mode as IL-1β[23–25]. This feature was confirmed under more physiological conditions by using two solution techniques, NMR and SAXS. On the basis of these results, it is highly likely that the left binding mode is the common mode in the IL-1 family; however, the IL-36/IL-36R/IL-1RAcP ternary complex structure has not been determined. Although the general binding mode was conserved, substantial differences were observed at the ligand-receptor or receptor-receptor interfaces in the IL-18 and IL-1β ternary complexes, which was expected based on the significant sequence deviations (Supplementary Fig. 1). The pronounced effects from such deviations include the unique compositions of secondary structure elements in IL-18Rα-D1 and IL-18Rs-D2, such as the lack of a β-strand that is typically conserved among Ig-like domains. This feature has led to the unique subdomain orientation of IL-18Rβ, and may partly explain why IL-1RAcP exhibits the promiscuous ligand recognition mode, although IL-18Rβ does not. On the basis of the presumable existence of d2 in IL-36R-D2 and the IL-36 (ref. 27) structure, it is likely that the IL-36 system also adopts the left binding mode with similar orientation to the IL-1β system.

Furthermore, we found a potential common trait among the IL-1 family, which is that the N-linked glycans presumably bridge two receptors in the ternary complex. Intriguingly, this feature was only observed in two functional ternary complexes (IL-1β/IL-1RI/IL-1RAcP and IL-18/IL-18Rα/IL-18Rβ) but was absent in the decoy ternary complex (IL-1β/IL-1RII/IL-1RAcP) and may contribute the binding affinity. Nevertheless, our SPR analyses showed that the difference in IL-18Rα-binding affinity for IL-18Rβ was only trivial even without glycosylation (N236Q^{Rα} in Table 2). This discrepancy may be due to the distinct sugar modification patterns between insects and mammals. N-glycans are mostly pauci-mannose (Fig. 6b, not greater than three MAN) oligosaccharides in silkworm[30], while mammals contain more varied outer sugar chains; certain chains are longer with more complicatedly mixtures (that is, MAN, NAG, galactose and sialic acid). Thus, larger interaction surfaces on N236^{Rα} sugar chains in humans are expected, which could strengthen the affinity. In contrast, one N-glycan chain likely plays a unique role in the IL-18 system, as the IL-18Rα Asn297^{Rα} sugar chain moderately interacts with IL-18 in both the binary and ternary complexes (Fig. 6d). In fact, IL-18Rα without the sugar chain (N297Q) exhibited a threefold lower binding affinity (Table 2). To our best knowledge, such sugar–ligand interactions have not been reported for other IL-1 family members. For the IL-1β complexes, any N-glycan chains on IL-1RI(RII) appear too distal to the ligand for direct contact.

IL-1 family activity *in vivo* are modulated by the counteractions of natural inhibitors, such as receptor antagonists (IL-1Ra, IL-36Ra and IL-38), soluble receptors (sIL-1RI, sIL-18R and

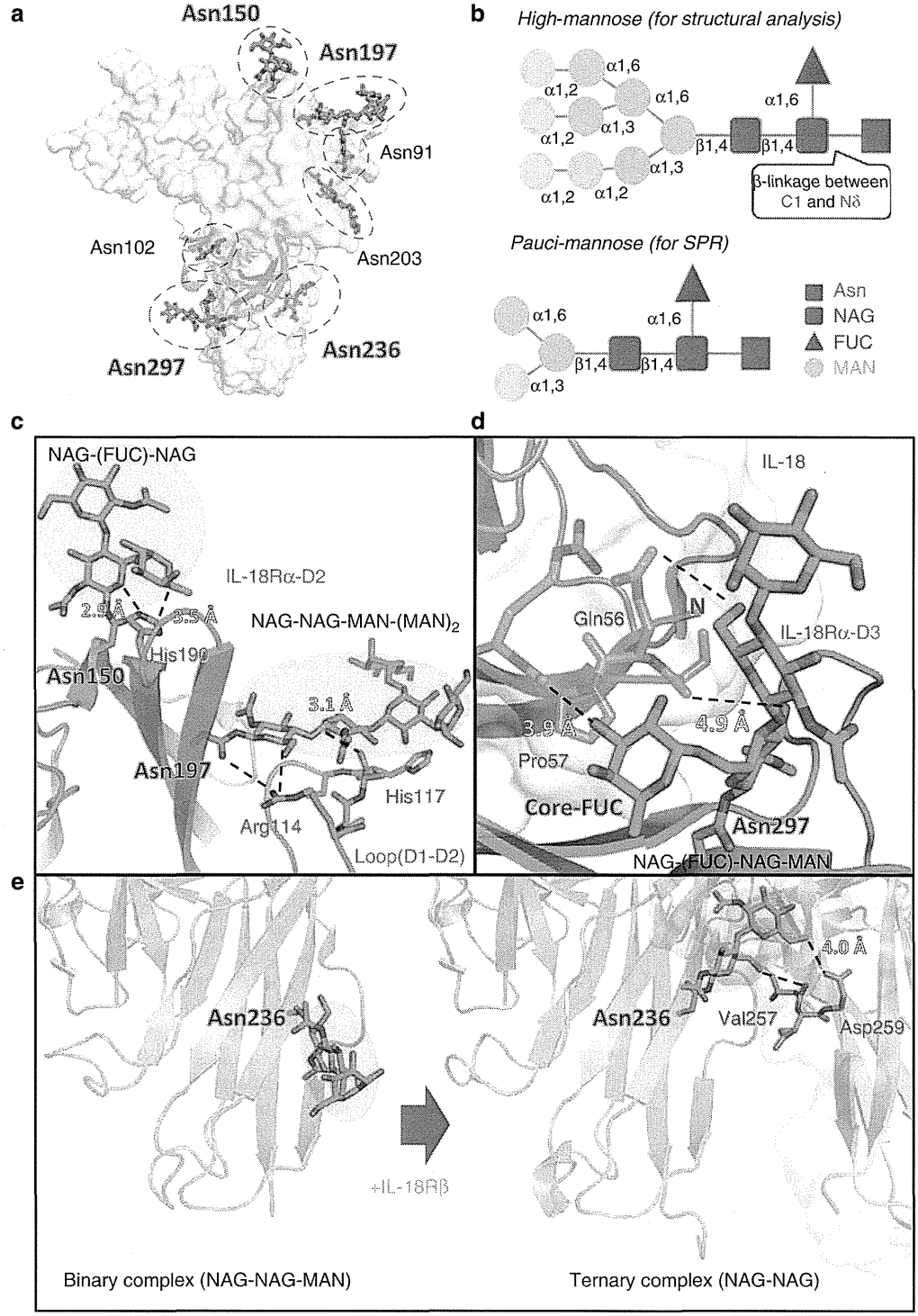

Figure 6 | The sugar contacts that maintain IL-18/IL-18Rα/IL-18Rβ. (**a**) The N-linked glycans identified from the structure. (**b**) The N-linked glycosylation in this study. (**c**) Intramolecular interactions between the carbohydrates on Asn150^{Rα} and His190^{Rα} as well as on Asn197^{Rα} and the D1-D2 loop. (**d**) Interactions between the N-linked carbohydrates on Asn297^{Rα} and IL-18. Core-FUC moderately interacts with IL-18 at an ~4 Å distance. (**e**) Interactions between the N-linked carbohydrates on Asn236^{Rα} and IL-18Rβ.

sST2) and IL-18BP. These proteins tightly bind their target cytokines or receptors, which impedes formation of ternary complexes that initiate intracellular signal transduction. This balancing feature facilitates secure control of inflammatory responses *in vivo*. Our structures not only demonstrate the receptors' molecular recognition mode for IL-18, but they also explain the IL-18 inhibitors' mechanism of action. Superimposition of the IL-18/IL-18Rα and IL-18/IL-18BPs complex structures[20,22] shows that the IL-18BP binding site on IL-18 precisely corresponds with the IL-18Rα-D3 binding site. Thus, IL-18BP clearly inhibits IL-18Rα binding through steric hindrance (Supplementary Fig. 8a). Recently, IL-37 (IL-1F7b) was proposed to function as an anti-inflammatory cytokine[31]. IL-37 weakly bound IL-18Rα with 50 times lower affinity than IL-18

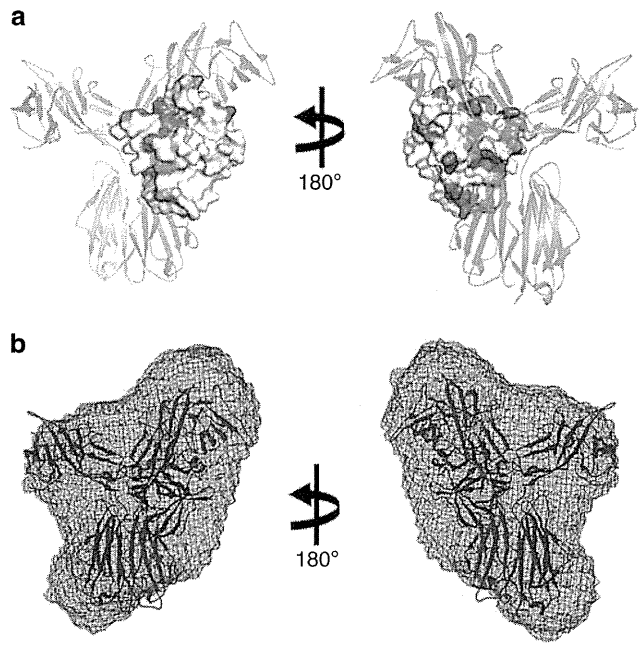

Figure 7 | The solution-state IL-18/IL-18Rα/IL-18Rβ binding mode. (**a**) The results of cross-saturation experiments with [^{2}H-^{15}N]-IL-18/IL-18Rα (forest) and the chemical shift change of [^{2}H-^{15}N]-IL-18/IL-18Rα on adding IL-18Rβ (orange) are coloured on the crystal structure of IL-18 in complex with IL-18Rα and IL-18Rβ. (**b**) Superimposition of the IL-18/IL-18Rα/IL-18Rβ crystal structure and the low-resolution SAXS envelope.

Table 2 | Functional epitopes of IL-18 and IL-18 receptors.

	K_d (10^{-8} M)
Ligand: IL-18Rβ WT	
Analyte: IL-18 mutant/IL-18Rα WT complex	
IL-18 WT(control)	1.5 ± 0.1
IL-18 G108A	No binding
IL-18 H109A	No binding
IL-18 D110A	5.6 ± 0.8
IL-18 K112A	No binding
IL-18 G145A	2.8 ± 0.1
IL-18 R147A	5.7 ± 0.3
IL-18 M150A	6.0 ± 0.5
Ligand: IL-18Rβ mutant	
Analyte: IL-18 WT/IL-18Rα WT complex	
IL-18Rβ WT (control)	1.5 ± 0.1
IL-18Rβ L167A	3.3 ± 0.4
IL-18Rβ E210A	32.7 ± 0.9
IL-18Rβ Y212A	No binding
IL-18Rβ Y214A	5.0 ± 0.5
IL-18Rβ K313A	10.9 ± 0.9
Ligand: IL-18Rβ WT	
Analyte: IL-18WT/IL-18Rα mutant complex	
IL-18Rα WT (control)	1.5 ± 0.1
IL-18Rα N236Q	1.7 ± 0.3
Ligand: IL-18Rα mutant	
Analyte: IL-18 WT	
IL-18Rα WT (control)	6.9 ± 0.2
IL-18Rα N297Q	25.8 ± 2.6

Ligand: the interactant captured on the sensor surface. Analyte: the interactant in free solution. WT: wild type. Values are the means ± s.d. of the results derived from three independent experiments.

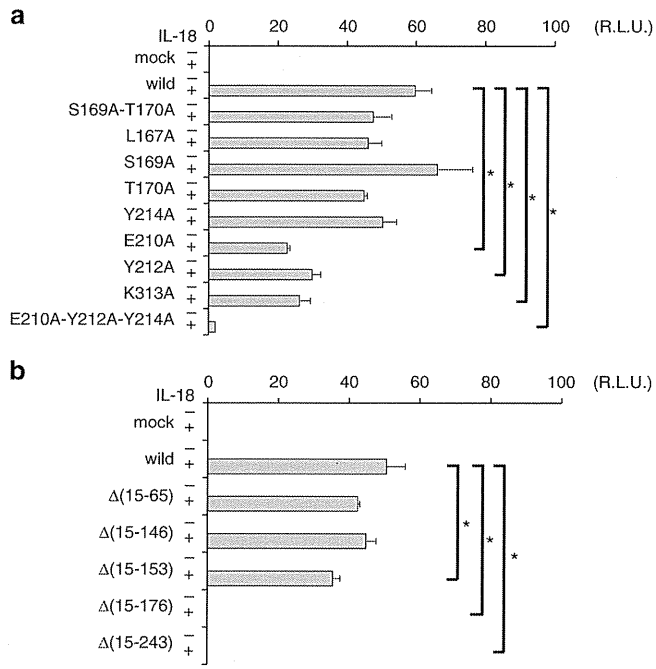

Figure 8 | The effect of mutations on protein-protein interfaces for signal transduction. Cell-based NF-κB activity assay for IL-18Rβ with (**a**) an alanine substitution and (**b**) N-terminal deletion. Each column indicates the relative luciferase activity unit (R.L.U.), for the stimulated cells(+) and the non-stimulated cells(−). The data are the mean ± s.d. for triplicate experiments. Asterisks inside the graphs indicate the significance from comparing mutant versus wild-type IL-18 Rβ, which was determined using a one-way ANOVA with Bonferroni's multiple comparison test; *$P<0.05$. This experiment is representative of three independent experiments.

(Fig. 2a), and did not activate signal transduction[32]. Consistent with this notion, the essential IL-18 amino acids for the IL-18Rβ interactions, as well as for IL-18Rα, determined in this study are not conserved in IL-37 (Supplementary Fig. 1a), which suggests that IL-37 is incapable of forming the ternary complex that enables signal transduction. In addition to the natural inhibitors, several anti-IL-18 antibodies have been developed for therapeutic purposes[21,33]. The structures herein clearly explain how these antibodies impede binding between the ligand and receptors (Supplementary Fig. 8b).

The molecular interface differences herein are important because they may provide numerous opportunities for designing molecules that specifically stabilize or interrupt IL-18 ternary complex formation without affecting other IL-1 family members. Unlike molecules that target more downstream signalling pathways, these molecules can be used to treat ligand-specific diseases and avoid side effects due to interference with common intracellular signalling pathways. The structural information collected in this work will facilitate development of an IL-18 modulator in multiple ways. For example, recombinant derivatives of IL-18, which bind to IL-18Rα more strongly relative to wild type of IL-18, can be logically designed based on the structures[34]. The structures will especially benefit small molecule design; small molecules are generally more cost effective once developed, and thus preferable to proteinous compounds. The data obtained in this study provide an atomic framework for molecular interfaces between IL-18 and receptors as well as between the two receptors, which serve as promising drug target sites, and hence will aid in development of effective IL-18 inhibitors.